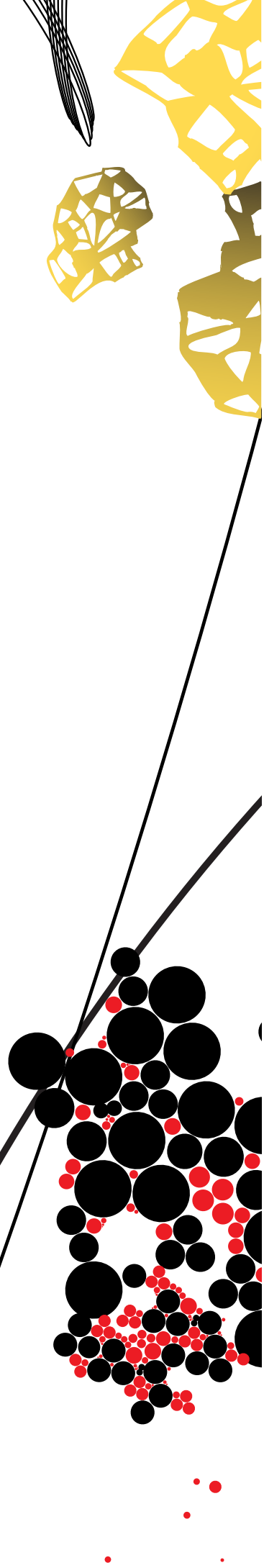

EEMCS Faculty

Power Electronics & EMC Group

Electrochemical Impedance Spectroscopy of Lithium-Ion Batteries: A Data-Driven Modelling Approach Using Distribution of Relaxation Times

Eduard Aguilar Boj

supervised by

PhD. Candidate Seyedreza Azizighalehsari

Dr.ir. Prasanth Venugopal

prof.Dr. Thiago Batista Soeiro

Master Thesis Project

April 2023

UNIVERSITY OF TWENTE.

Electrochemical Impedance Spectroscopy of Lithium-Ion Batteries: A Data-Driven Modelling Approach Using Distribution of Relaxation Times

Eduard Aguilar Boj
Power electronics & EMC
University of Twente
Enschede, Netherlands
e.aguilarboj@student.utwente.nl

Abstract—Lithium-ion batteries have a significant role in storing and using energy, an increasing market led by the electrification of transportation. Developing reliable and accurate models for lithium-ion batteries is crucial for optimizing their performance and assure they are working in optimal conditions, minimizing the ageing and degradation they experience in the cycling process. In this project, several lithium-ion batteries aged under different conditions, C-rate, Temperature and ΔDoD, were measured using Electrochemical Impedance Spectroscopy (EIS). The acquired data was processed using the proposed algorithm based on the Distribution of Relaxation Times (DRT) analysis. The inclusion of DRT analysis in the processing algorithm produced more consistent fitting results for the Equivalent Circuit Model (ECM) with less variability between measurements. A preliminary study was also conducted to investigate the correlations between the changes in the ECM and the cycling conditions of the cell. The results of this project demonstrate the potential of DRT analysis as a dataset processing method to improve the accuracy and reliability of lithium-ion battery models.

Keywords—Lithium-ion batteries, Electrochemical Impedance Spectroscopy, Ageing, Distribution of Relaxation Times, Equivalent Circuit Model

CONTENTS

List of Acronyms 2

1 Objectives 2
1.1 Thesis Outline 3

2 Introduction 3
2.1 Electrical Properties 3
2.1.1 Voltage 3
2.1.2 Voltage Limits 3
2.1.3 Capacity 4
2.1.4 C Rate 4
2.1.5 ΔDepth of Discharge 4
2.1.6 Impedance 4
2.2 Thermal Properties 6
2.2.1 Heat Generation . . . 6
2.2.2 Thermal Runaway . . 6
2.3 Chemical Properties 6
2.3.1 Anode 6
2.3.2 Electrolyte 6
2.3.3 Cathode 7
2.4 Battery Degradation and Ageing Mechanisms 7

3 Electrochemical Impedance Spectroscopy datasets 8
3.1 External datasets 8
3.1.1 University of Cambridge 8
3.1.2 Sandia national lab . 8
3.1.3 Oxford 9
3.1.4 Stanford University . 9
3.1.5 University of Warwick 9
3.1.6 NASA 9
3.1.7 Wisconsin-Madison & McMaster University 10
3.2 University of Twente 10

Part of this master thesis has been published in the conference ICPE 2023-ECCE Asia

3.2.1 Data collection justification 10
3.2.2 University of Twente dataset 10
3.3 Comparison 10

4 Analysis Methodology 11
4.1 Electrochemical Impedance Spectroscopy 11
4.2 Distribution of Relaxation Times 12
4.3 Equivalent Circuit Models . . . 14
4.4 Accuracy comparison 15

5 Results and Discussion 15
5.1 Cambridge Dataset 16
5.1.1 Dataset selection and cleanup 16
5.1.2 DRT: Peak selection and ECM 17
5.1.3 Least Squares Fit . . . 17
5.1.4 Data Correlations and Trends 17
5.2 Twente Dataset 18
5.2.1 Dataset selection and cleanup 18
5.2.2 DRT: Peak selection and ECM 19
5.2.3 Least Squares Fit . . . 20
5.2.4 Data Correlations and Trends 20

6 Conclusions 20

7 Limitations and Recommendations 21

References 23

Appendix A: Experimental set-up 26
A.1 Tested battery 26
A.2 Cycling equipment 26
A.3 Cycling protocol 26

List of Acronyms

ΔDoD ΔDepth of Discharge.
BoL Beginning of Life.
CC Constant Current.
CC-CV Constant Current-Constant Voltage.
CPE Constant-Phase Element.
DRT Distribution of Relaxation Times.
ECM Electrical Equivalent Model.
EIS Electrochemical Impedance Spectroscopy.
EMI Electromagnetic Interference.
EOL End Of Life.
ESW Electrolyte Stability Window.
LAM Loss of Active Material.
LCO Lithium Cobalt Oxide ($LiCoO_2$).
LFP Lithium Iron Phosphate ($LiFePO_2$).
LIB Lithium-Ion Battery.
LLI Loss of lithium inventory.
LMO Lithium Manganese Oxide ($LiMn_2O_4$).
LQF Least Squares Fit.
NASA National Aeronautics and Space Administration.
NCA Lithium Nickel Cobalt Aluminium Oxide ($LiNiCoAlO_2$).
NMC Lithium Nickel Manganese Cobalt Oxide ($LiNiMnCoO_2$).
OCV Open Circuit Voltage.
ppd Points Per Decade.
SEI Solid Electrolyte Inter-phase.
SoC State of Charge.
SoH State of Health.

1 Objectives

This thesis aims to develop a reliable and accurate model for lithium-ion batteries by incorporating various factors influencing their performance, such as ageing and cycling conditions. The primary focus is on using Electrochemical Impedance Spectroscopy (EIS) data and Distribution of Relaxation Times (DRT) analysis to enhance the consistency and reliability of Equivalent Circuit Models (ECM). The ultimate goal is to optimize the performance and extend the lifespan of lithium-ion batteries across multiple applications.

- Conduct a literature review on different lithium-ion battery modelling approaches, focusing on utilizing Electrochemical Impedance Spectroscopy (EIS) and Equivalent Circuit Models (ECM).
- Age several lithium-ion batteries under different ambient conditions and measure their impedance variations over time using EIS.
- Develop a data processing algorithm that improves the consistency and reliability of ECM fitting results.
- Investigate the correlations between changes in the ECM parameters and the cycling conditions of the lithium-ion battery cells.

1.1 Thesis Outline

Chapter 2 provides a general introduction to lithium-ion batteries, discussing their significance, the need for research in this area, and basic concepts related to their modelling. Chapter 3 presents an overview of the available datasets containing EIS measurements, their locations, and an evaluation of whether the data aligns with the research objectives. Chapter 4 details the proposed analysis methodology, ranging from the EIS configuration to the examination of the fitted parameters in the ECM. In Chapter 5, the outcomes of applying the analysis methodology to the selected datasets are presented. Chapter 6 summarizes the research conclusions, while Chapter 7 highlights the study's limitations and provides recommendations for future work.

2 Introduction

Developing improved energy storage technologies is one of the critical objectives of meeting the various global decarbonization agreements, such as the Paris Agreement. Most of the pressure in the near future will come from the transition to electricity-based mobility, as reflected in figure 1.

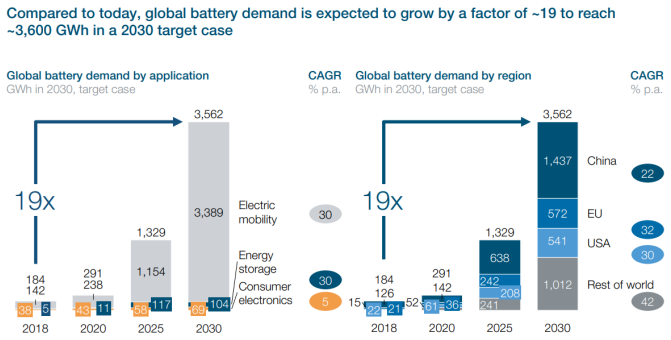

Fig. 1. Global battery industry growth by application and region by 2030, from [1].

Currently, the best alternative to fossil fuels for storing energy is dominated by the Lithium-Ion Batteries (LIBs), as they have a high energy density, low self-discharge, and no memory effect [2]. LIB are an electrochemical construct encompassing different chemicals that achieve energy storage [3].

The performance of batteries is heavily influenced by the dynamic operating conditions they undergo. The non-linear and time-varying characteristics of battery behaviour during operation pose a significant challenge in accurately determining the underlying chemical processes. A noticeable miss exists between the electrochemical phenomena and the circuit model used to infer these processes within the battery [4].

In this thesis, batteries are studied from the electrical engineering point of view, not entering into the chemical implications of the different findings. Even though a base understanding of how these batteries are built is needed to understand some of the electrical degradation processes observed, given that, in the following sections of this chapter, there will be an introduction to the electrical properties, the thermal properties, and the chemical properties that encompass LIBs, as well as the modelling and analysis techniques that will be used.

2.1 Electrical Properties

Lithium-ion batteries exhibit several electrical properties, such as voltage, current, capacity, and internal resistance, which are critical to their operation and performance. This section will provide an overview of these properties, establishing the context necessary for understanding this thesis's modelling and analysis techniques.

2.1.1 Voltage

The voltage of a lithium-ion battery, also known as the cell potential, is the driving force that propels the flow of electrical charge between the battery's electrodes. The voltage primarily depends on the battery's State of Charge (SoC) and the electrode materials of electrochemical potentials. Fig. 2 represented a typical distribution of the change in the voltage a battery has dependent on their SoC With

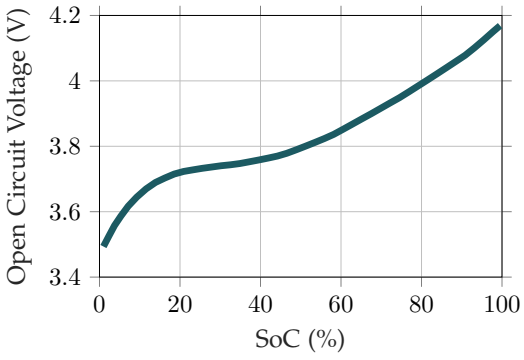

Fig. 2. OCV curve of a Lithium-ion cell

the help of a good model of the battery behaviour and keeping under a specific operating range.

2.1.2 Voltage Limits

Voltage limits are crucial for lithium-ion batteries' performance, safety, and longevity. These limits define the safe operating range, with the lower voltage

limit preventing excessive lithium-ion extraction and the upper limit avoiding overcharging. Adhering to the specified voltage limits helps maintain optimal performance and extend battery life during charging and discharging cycles [5].

2.1.3 Capacity

Capacity is a measure of the total amount of electrical energy a battery can store and deliver. Expressed in ampere-hours (Ah) or watt-hours (W·h), capacity is determined by the amount of active material in the battery and the efficiency of the electrochemical reactions occurring within the cell.

2.1.4 C Rate

The C rate measures a battery's charge or discharge rate, expressed as a multiple of its capacity. A higher C rate implies a faster charging or discharging process, while a lower C rate indicates a slower one. For example, a 1C rate means the battery will be charged or discharged in one hour, while a 0.5C rate extends the process to two hours. The choice of C rate is crucial for balancing performance, efficiency, and battery life, as faster rates can lead to increased heat generation and reduced cycle life [5].

2.1.5 ΔDepth of Discharge

The ΔDepth of Discharge (ΔDoD) is a term that has different uses in the battery area of knowledge. In this master thesis, it will be used to describe the difference between the maximum SoC and the minimum SoC that the cycling profile of a cell achieves.

2.1.6 Impedance

Impedance is a key parameter characterizing the opposition to the flow of electrical current within a battery. Factors contributing to internal resistance include electrolyte conductivity, electrode material, and contact resistance between electrodes and current collectors. In the complex plane, impedance has two components: resistance (real) and reactance (imaginary). Battery impedance depends on various operating conditions, such as temperature, SoC, and current [6]. Variations in impedance can lead to permanent degradation in the cell (ageing), emphasizing the importance of maintaining optimal operating conditions to ensure the battery's longevity and power delivery capabilities.

2.1.6.1 Basic Impedance Elements: To model the complex impedance behaviours of batteries, basic circuit elements are combined, approximating the observed impedance characteristics. These elements include resistors, capacitors, inductors, RC circuits, Constant-Phase Elements (CPEs), and Warburg elements. While these elements help to model the impedance behaviour of batteries, they do not necessarily represent the actual internal components of the battery.

All the formulas of this section are given relative to the angular frequency:

$$\omega = 2\pi f \tag{1}$$

2.1.6.2 Resistor: Ideal resistors are the simplest impedance element, their current is always proportional to the voltage, so there is no phase shift (reactive part).

$$Z(\omega) = R \tag{2}$$

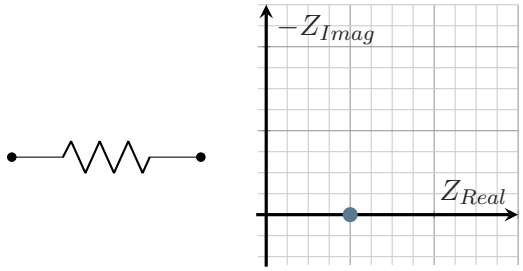

Fig. 3. Electrical symbol of a resistor with the impedance spectrum it produces in a frequency sweep.

2.1.6.3 Capacitor: Ideal capacitors are pure reactive elements, have zero resistance, and their magnitude is inversely proportional to the frequency.

In the Nyquist plot, a pure capacitive behaviour appears as a vertical line fixed at $Z_{re} = 0$, and the imaginary component tends to be infinite as the frequency decreases.

$$Z(\omega) = \frac{1}{jC\omega} \tag{3}$$

2.1.6.4 Inductor: An ideal inductor is the opposite of an ideal capacitor. They also have negligible restive component, but their reactive effect makes the voltage lead the current by a phase shift of 90º, viewed in the Nyquist plot as a vertical line (down in the representation used in this research, as the major capacitive effect that have the batteries

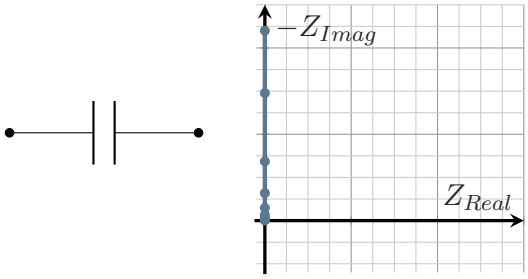

(a) (b)

Fig. 4. Electrical symbol of a capacitor with the impedance spectrum it produces in a frequency sweep.

makes it standard to work with the imaginary axis inverted)

$$Z(\omega) = Lj\omega \tag{4}$$

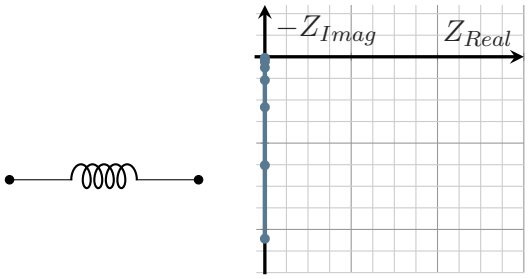

(a) (b)

Fig. 5. Electrical symbol of an inductor with the impedance spectrum it produces in a frequency sweep.

2.1.6.5 RC Circuit: In the chapter

2.1.6.6 Series:

$$Z(\omega) = Z_R(\omega) + Z_C(\omega) = R + \frac{1}{jC\omega} \tag{5}$$

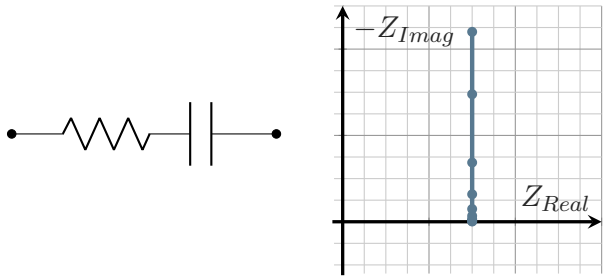

(a) (b)

Fig. 6. Electrical symbol of a series RC pair with the impedance spectrum it produces in a frequency sweep.

2.1.6.7 Parallel:

$$Y(\omega) = \frac{1}{Z(\omega)} = \sum_n \frac{1}{Z_n(\omega)} \tag{6}$$

$$Z(\omega) = \frac{R}{1 + j\omega RC} \tag{7}$$

$$\tau = RC \tag{8}$$

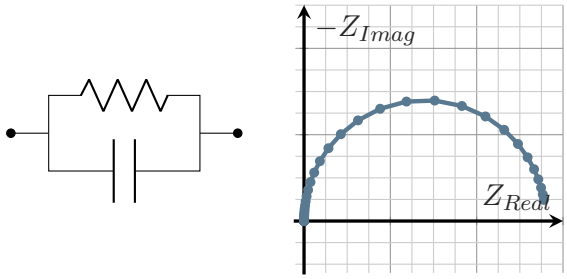

(a) 1st caption (b) Nyquist plot

Fig. 7. Electrical symbol of a parallel RC pair with the impedance spectrum it produces in a frequency sweep.

2.1.6.8 Constant Phase Element: Contrary to the other impedance elements presented in the section, the CPE is a theoretical construct to explain an impedance behaviour that does not have an electrical ideal equivalent.

The CPE is used to describe processes that behave as an in-between an ideal capacitor (phase sift = $\frac{\pi}{2}$) and an ideal resistor (phase shift = 0°).

$$Z(\omega) = \frac{1}{Q(j\omega)^\alpha} \tag{9}$$

where:

Q = Capacitance or Conductance
α = number of waves

these elements can be rearranged as:

$$\begin{aligned} Magnitude \quad |Z_{cpe}(\omega)| &= \frac{1}{Q\omega^\alpha} \\ Phase\ shift \quad \phi_{cpe} &= \frac{-\alpha\pi}{2} \end{aligned} \tag{10}$$

$$\tau = (RQ)^{1/\alpha} \tag{11}$$

In the case, $\alpha = 1$ the CPE will behave as an ideal Capacitor and in the case, $\alpha = 0$ the behaviour of the CPE will be the same as an ideal resistor [7, Chapter 14].

2.1.6.9 Warburg Element: A special case of a CPE is the Warburg element when $\alpha = 0.5$.

$$Z(\omega) = \frac{W}{\sqrt{\omega}} - j\frac{W}{\sqrt{\omega}} \tag{12}$$

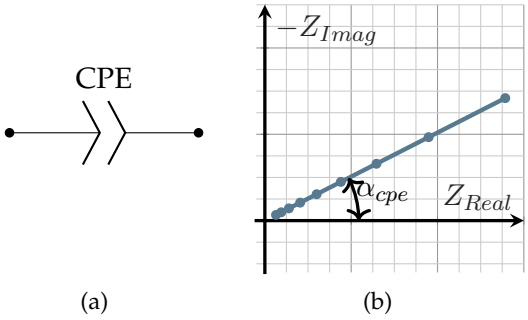

Fig. 8. Electrical symbol of a CPE with the impedance spectrum it produces in a frequency sweep.

2.2 Thermal Properties

2.2.1 Heat Generation

During the operation of a LIB, heat is generated as a result of various factors, including electrical losses, chemical reactions, and mechanical friction within the cell. The thermal behaviour of a cell can be used as an indicator of the health of it. With the ageing process and the increase of impedance the cells cycle at higher temperature then at their Beginning of Life (BoL). In some applications thermal management may be key to assure the correct behaviour of the system.

2.2.2 Thermal Runaway

Thermal runaway is a condition in which an exothermic reaction within a LIB causes a rapid increase in temperature, leading to a self-sustained cycle of increasing temperature and heat generation. This process can result in catastrophic failure, fire, or battery explosion.

Several factors can contribute to thermal runaway; including overcharging, over-discharging, excessive current, high operating temperature, and external short circuit. The chance of a thermal runaway can be minimized through careful battery design, effective thermal management systems, and the use of safety features such as thermal fuses.

2.3 Chemical Properties

Simplifying a battery to its more elemental form, it is formed by three elements; an anode, a cathode, and an electrolyte. By convention, the electrodes are named by their behaviour during the discharge phase of the battery, being the cathode one with a higher potential and the anode one with the lower one. [8, Chapter 1]. The term LIBs does not refer to a unique chemistry, but to a family of chemistries that share the use of lithium-ion in an alloy (usually in the cathode) to store the energy [9]. In the figure 9, we can see different chemistries used for the battery electrodes, being for commercially available LIBs, new proposed LIBs chemistries or chemistries used on batteries not related with LIBs.

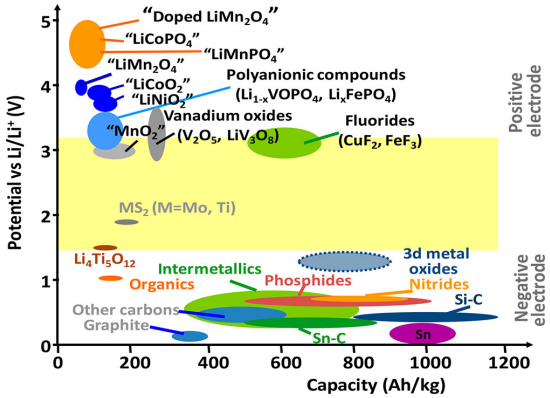

Fig. 9. Relationship between the potential and capacity of active materials utilized in Lithium-ion technologies [10], [11].

But what makes a good battery is not only the theoretical potential that a specific chemistry can achieve but a trade-off between life expectancy, performance, safety, cost, and other considerations that only the final application can determine the most suitable.

2.3.1 Anode

In anode materials, there is not much of a discussion, as most of the commercial batteries use carbon/graphite; carbon offers a favourable combination of factors such as reasonable pricing, plentiful supply, decent energy, and power density, and extended service life, making it more advantageous than other intercalation-based anode materials [5]. A more in deep study about the carbon anode can be found in [12] where a comparison between the different crystalline structures of carbon is made to compare the differences in charge storage capabilities.

2.3.2 Electrolyte

The electrolyte is a material inside the battery that has to be electrically insulating but a good conductor of ions[5]. The Open Circuit Voltage (OCV) values, which is the potential difference between the positive and negative electrodes, have to be maintained inside Electrolyte Stability Window (ESW), which is the reason why LIBs have to be maintained over a minimum voltage.

The importance of the electrolyte in this thesis is that in the interface between the electrolyte and

the electrodes, as a bi-product of the redox reactions that enable the battery to operate, a crystalline structure grows called Solid Electrolyte Inter-phase (SEI). This is one key degradation parameter that affects the electrical behaviour of the battery.

Once the SEI layer is formed, the reaction between the electrodes and the electrolyte is diminished, hindering the battery degradation. Battery performance, irreversible charge loss, rate capability, cycle ability, or safety are parameters affected by the SEI composition [13]. Thus, additives are introduced in the electrolyte to control the chemical structure of this layer [14].

Its effects on the electrical characteristics will be explained in section 2.4

2.3.3 Cathode

There are several cathode chemistries currently used in the market, and it is usually by an acronym of these chemistries that the cells are refereed. The cathode chemistry induces differences in cell performance such as max current that the cell can provide, max charge, degradation over ageing, etc. Thus, the best chemistry will depend on the application.

Some common cathode materials include:

- **Lithium Cobalt Oxide ($LiCoO_2$) (LCO):** LCO offers high energy density but has lower thermal stability. The cost can be a factor due to its cobalt content. These batteries are commonly found in portable electronic devices such as smartphones, laptops, and cameras [5].
- **Lithium Manganese Oxide ($LiMn_2O_4$) (LMO):** LMO cathodes are known for their high thermal stability, making them a safer option compared toLCO. However, they have lower energy density and a shorter cycle life. These batteries are often used in power tools and electric vehicles [5], [15].
- **Lithium Iron Phosphate ($LiFePO_2$) (LFP):** LFP cathodes offer excellent thermal stability, safety, and long cycle life but have a lower energy density. They are commonly used in electric vehicles, energy storage systems, and various industrial applications [5], [16].
- **Lithium Nickel Manganese Cobalt Oxide ($LiNiMnCoO_2$) (NMC):** NMC cathodes provide a good balance of energy density, thermal stability, and cost, making them popular for use in electric vehicles and energy storage systems. Different ratios of nickel, manganese, and cobalt can be adjusted to optimize specific characteristics [5], [17].
- **Lithium Nickel Cobalt Aluminium Oxide ($LiNiCoAlO_2$) (NCA)):** NCA cathodes have high energy density, good cycle life, and relatively low cost due to their lower cobalt content. They are often used in electric vehicles and energy storage systems [5], [18].

2.4 Battery Degradation and Ageing Mechanisms

When the battery is in use, different chemical reactions occur between the other components that allow energy extraction (or injection) into the system. Unfortunately, there are non-desirable effects that are unavoidable (at least with current chemical formulations) that modify the battery operation characteristics. These effects can be grouped into temporal, which will contain how the chemical reactions change based on the temperature, current demand, humidity..., and permanent, which are the sum of the different degradation processes taking place in the battery. To make it more complex, all these effects depend on the chemistry, and each reacts differently to a modification of the operation conditions.

The degradation process refers to the non-reversible part of the chemical reactions in the battery. After every charge-discharge cycle, there is a part of the material loss converted to a different element. This not only accumulates after every cycle, making the battery less capable of performing as in the beginning, but also its presence modifies the electrical behaviour of the battery. The accumulation of this permanent degradation process is what constitutes the ageing of the battery.

This project aims to examine battery degradation from an electrical perspective, focusing on the cumulative impact of ageing processes on electrical properties rather than investigating each process in detail.

In Fig. 10, the most prominent ageing mechanisms occurring in the anode, cathode, and other active materials are depicted, along with their primary contributions to either capacity fade or increased impedance. This visual representation aims to clearly understand the relationship between various degradation processes and their effects on the battery's performance.

Loss of lithium inventory (LLI) refers to the irreversible trapping of lithium ions in inactive materials or side reactions, reducing the number

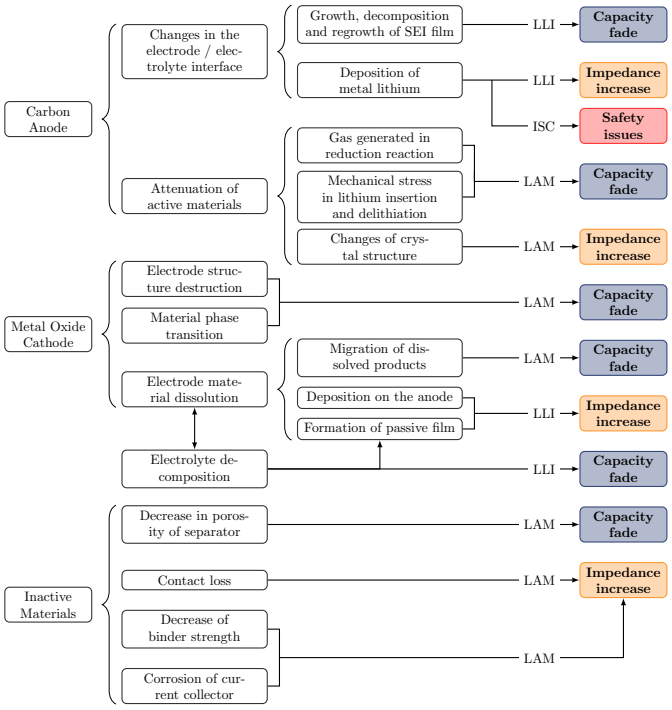

Fig. 10. Predominant mechanisms of ageing that arise within a battery's anode, cathode, and other active materials. The diagram outlines the primary factors that contribute either to capacity degradation or heightened impedance [19].

of available lithium ions for energy storage.Loss of Active Material (LAM) occurs when the active materials in the anode or cathode degrade, leading to reduced energy storage capacity. Both LLI and LAM contribute to capacity fade, which is the decline in the battery's ability to store energy over time.

On the other hand, increased impedance results from the SEI layer's growth on the anode, the formation of passivating layers on the cathode, and other degradation processes that hinder ion transport within the battery. This increase in impedance reduces the battery's efficiency, ultimately affecting its overall performance.

By understanding the relationship between these ageing processes and their effects on battery performance, this project aims to provide valuable insights into the electrical properties of battery degradation.

3 Electrochemical Impedance Spectroscopy Datasets

A great effort has been made to sort most of the available datasets with information relating to cycling batteries in [20]. Despite being one-year-old, differences in how the data can be accessed have been found. In this section, similar to in the cited paper, there will be an overview of the datasets found, focusing on the ones containing Electrochemical Impedance Spectroscopy (EIS) measurements; there will be an introduction of the purpose of that data collection, a resume of the data format and a value judgment of the fitness of the data for the purpose of this research. Finally, a table comparing the different datasets can be found in Tab.1. In the section 3.2, it will be introduced why it is relevant to have our own dataset and how we are making the measurements.

3.1 External datasets

3.1.1 *University of Cambridge*

The dataset was collected for the study of the publication [21], where the aim was to train a neural network to predict the state of the battery having impedance measurements as an input. The data can be downloaded from [22]. The data collection was performed over LCO LR2032 coin LIB cells. The set consists of 12 batteries cycled at 1C Constant Current-Constant Voltage (CC-CV) charge protocol and 2C discharge at Constant Current (CC), 8 cells are cycled at 25°, 2 cells are cycled ad 35° and 2 cells are cycled at 45°. The End Of Life (EOL) is defined at 80% of the initial capacity, which happened between 250 and 300 cycles. There are EIS measurements at 9 points of the charge/discharge profile at each cycle, making this dataset of about 20000 measurements. From those, only about 9000 measurements are usable for our project (measurements taken place in the measurement location I, V, and IX) as the other six were obtained without sufficient resting or with current in the cells. More information about the measurement points and condition of the cells at that state can be found in the "additional information" part of the cited paper.

3.1.2 *Sandia national lab*

The Sandia national lab has different datasets with measurements on cycling batteries. From those, there are two with EIS data that are relevant to mention.

The first dataset, "Battery Cell Testing Data Archive", can be downloaded from [23] and was published with this paper [24] explaining the test procedure. The test is performed on 24 cells of four different chemistries, LCO,LFP,NCA, and NMC. Each cell is cycled at 1C CC-CV charge protocol and discharged with all the different CC profiles,

discharges at 1C, 5 discharges at 5A, and 5 discharges at 10A; if the chemistry allows it there are 5 discharges at 20A and 5 discharges at 30A. This test is done at a constant temperature of 5º, 15º, 25º, 35º, or 45 °C, having different cells for each temperature. The EIS measurements took place at the BoL of the cell, before the test and after this test was performed. Even though the test procedure does not adapt to the data needed for the analysis proposed in this paper, the documentation provided about the test set up, test conditions, and cells examined is worth mentioning as a reference of good practices.

The second dataset is a more ambitious data collection that was published in [25] explaining the test procedure. The test was done in 18650 cells of three different chemistries: 30 cells of LFP (1.1 Ah), 24 cells of NCA (3.2Ah), and 32 cells of NMC (3Ah). A full description of the cells is available in the cited paper. The cells are cycled at three different temperatures, 15º, 25º and 35º, three different ΔDoD, 0% to 100%, 20% to 80%, and 40% to 60% and discharged at four different C rates, 0.5C, 1C, 2C and 3C. Making 12 cycling condition groups were at least 2 cells of each chemistry had been cycled. The study concluded once a cell reached 80% of its initial capacity. After contacting them we have confirmed that at the moment of writing this thesis only the cycling data has been publicly released in [26] but the EIS measurements have still not been disclosed; expecting to be in 2023 after the publication of a paper analysing the data.

3.1.3 Oxford

The University of Oxford has a battery intelligence lab that has different battery data published on their website as well as in the Battery Archive project [26]. The dataset containing publicly available EIS data, 'Path Dependent Battery Degradation dataset', is divided into three parts that can be found in [27]–[29]. The test was performed to 12 Panasonic NCA 18650 LIBs. Mixing cycling profiles at C/2 and C/4 rate with CC-CV protocol for charging and CC load for discharging and calendar ageing rests of 10 days or 2 days; sorting the batteries in 4 groups of cycling environments. The ΔDoD is in all the cases from 100% to 0%. The EIS measurement was only taken at three points during the test, at the BoL, at a middle point, and at the EOL. The end-of-life point is not defined in the test, but it is mentioned that the middle was at 384 days of cycling. EIS was performed at 80%, 50% and 20% SoC. It is mentioned that the EIS resolution is of 6 Points Per Decade (ppd), but no information at which exact frequency is carried each of the different impedance measurements is provided.

For the analysis methodology proposed in this master thesis, it is needed to know the frequency measurement points, so this dataset was discarded for further analysis. Also, more EIS measurement points would be interesting to study and model the impedance change through the ageing.

3.1.4 Stanford University

The dataset was collected for the study of the paper [30] and the data can be downloaded from [31]. The test was performed on 10 21700 NMC cells following the Urban Dynamometer Driving Schedule discharge driving profile, with different CC-CV charge rates, from C/4 to 3C. All cells were tested on the same temperature (23º).

This discharging profile differs from the analysis intention of this work, centred in cells under constant cycling conditions. Even though the data is in good shape to be processes with our methodology, it was decided not to include it in this thesis as the circling conditions differed too much from the data gathered or the other analysed dataset.

3.1.5 University of Warwick

The University of Warwick made a dataset in cooperation with Jaguar in 2016 to study the viability of EIS technique to quantify the degradation of batteries in comparison with traditional methods[32], [33]. The data is stored in [34] where the cycling conditions are explained. The dataset is compounded of 4 NCA 18650 cells with a capacity of 3Ah. The cells were cycled at 25º with a ΔDoD of 100% at 1C CC-CV in the charging phase and discharged at a constant rate of 1C. The test ended after 500 cycles, with a characterization test (EIS measurement) every 50 cycles. The cells went through a pre-ageing process of 0, 50, 100, and 150 cycles before the start of the test. The cells were selected to have similar impedance (between 25%) and capacity (between 9%) before the start of the pre-ageing process.

Even though in [20] is listed as accessible upon request, after requesting access to the university we were informed that the data was collected under confidentiality agreements and could not be shared.

3.1.6 NASA

Recently, the National Aeronautics and Space Administration (NASA) website has been renewed, and the datasets link provided in [20] doesn't work any more. Despite that, the data is still accessible under the same link through the web. archive

project, which stores portions of the World Wide Web to ensure the information is preserved. The new location of the data is the one found in the references of this paper.

The first dataset NASA has *dataset 5. Battery dataset*[35] is not known, the purpose of this data collection. The dataset contains 34 18650 "commercial Li-ion" batteries, without referencing the exact chemistry/ies or reference to which batteries are. The cell's nominal capacity is 2000 mAh. The cells are cycled under the defined EOL criteria of 70% of its original capacity, under three temperatures (4º, 24º and 43º), charged at .75C with CC-CV protocol and with different discharge profiles encompassing .5C, 1C, and 2C CC and one group of 4 cells discharged at 2C square wave at 50% duty cycle. The EIS measurement is carried out in a frequency sweep between 0.1Hz to 5kHz. No information at which exact frequency is carried each of the different impedance measurements is provided. Assuming that the measurement was taken at equally logarithmic spaced points, we could calculate the freq data, needed for the analysis techniques we aim in this publication. With that assumption, we can say that the measurements were taken at 12 ppd.

The second dataset NASA has on battery data, *dataset 11. Randomized Battery Usage*[36] and was produced for the publication [37]. Even though in [20] is claimed to have EIS measurements, those could not be found in the downloadable data. There is also no reference of EIS or impedance measurements on the published paper that explains the dataset cycling conditions. NASA also has two other datasets regarding battery measurements, dataset 15 and dataset 16, but in them, no EIS measurement was taken.

3.1.7 Wisconsin-Madison & McMaster University

This dataset available in [38] carried out a different number of tests where the EIS at different temperatures and different SoC is performed. It is not clear, to our knowledge, which of the EIS measurements correlates to each of the claimed SoC points nor which ageing the battery reached the EIS test (pristine or continuation of the previous test). The dataset contains 'n' different 18650 NCA batteries that appear to have been cycled under an HPPC test before being tested at 25º, 10º, 0º, -10º and -20º and at intervals of 5% of SoC. Analysing the dataset, there are no 20 EIS measurements in each temperature and no information as to which of the different SoC are the ones saved in the dataset.

3.2 University of Twente

3.2.1 Data collection justification

Even though some research institutions are working with EIS data, the availability of those is scarce. One reason is that collecting EIS data is costly due to the long duration of the tests and the cost of the equipment, and sometimes the test is done in companion with companies that hide the data under non disclose agreements as happens with the Warwick dataset; another reason is that even the data is made public this is not properly documented, making the analysis of these either impossible or with lots of assumptions, as happens with the data of the University of Wisconsin.

Currently, only one public dataset, provided by the University of Cambridge, meets the quality requirements for this project. But that dataset only covers differences in ageing and temperature. Leaving out other interesting study cases as ΔDoD, C-rate, different chemistries, Electromagnetic Interference (EMI). Given the situation, it is interesting to build our own dataset to study the degradation of cells under different conditions. This also opens the possibility of making a contribution and ending up releasing the dataset.

3.2.2 University of Twente dataset

The dataset is only available internally in the EPEMC group, intending to release it in the future once it is completed. The data collection started for this master thesis and a full explanation of the test procedure can be found in Appendix A.

The dataset comprises 8 NCA 18650 with a nominal capacity of 2.6Ah. The cells are cycled under the defined EOL criteria of 80% of its original capacity. The test was carried out at room temperature (monitored to be 22ºC$\pm$1), charged at 1C with CC-CV protocol and with different discharge profiles encompassing 1C, 2C, 3C and 4C CC and three different ΔDoD, 20% to 100%, 20% to 80% and 40% to 80%. The EIS measurements are performed at 0% SoC, after the capacity measurement is performed every 10 cycles. With a frequency range from 10mHz to 100kHz at 10ppd

Before the release, this dataset is planned to be enlarged with different temperatures, chemistries and more cells per cycling condition.

3.3 Comparison

In the table 1 there is a resume of the main characteristics of the described datasets. In it, we can see the different cycling conditions. The experiment

TABLE 1
A comprehensive comparison of various EIS datasets.

Data set	Nr. of cells	Form fac.	Chem.	Year	Temp	Test end	ΔDoD	C-rate	Nom. cap. [mAh]	EIS SoC meas.	EIS range	nr. EIS meas.
U. of Twente	8	18650	NMC	2023	22°	SoH 80%	80-20% 100-0% 60-40%	1C 2C 3C 4C	2600	0%	0.01Hz-20kHz	-
U. of Cambridge [22]	12	LR-2032	LCO	2020	25° 35° 45°	SoH 80%	100-0%	2C	45	0% 100%	0.02Hz-20kHz	20000 (9000)
Sandia Lab. A [24]	24	18650	LCO LFP NCA NMC	2017	5° 15° 25° 35° 45°	no ageing	100-0%	1C 5A 10A 20A 30A	2500 1100 2900 3000	0%	0.1Hz-100kHz	126
Sandia Lab. B	86	18650	LFP NCA NMC	2020	15° 25° 35°	SoH 80%	100–0% 80–20% 60–40%	0.5C 1C 2C 3C	1100 3300 3000	n/a	n/a	n/a
Oxford [27]–[29]	12	18650	NCA	2020	24°	n/a	100-0%	C/2 C/4	3000	20% 50% 80%	0.01Hz to 5kHz	298
Stanford U. [31]	10 (6)	21700	NMC	2022	23°	SoH 80%	100-0%	HPPC	n/a	20% 50% 80%	0.01Hz-10kHz	53
Warwick U. [34]	4	18650	NCA	2016	25°	500 cycle	100-0%	1C	3000	20% 50% 90%	0.01Hz-100kHz	n/a
NASA 5 [35]	44	18650	n/a	2008	room	SoH 70%	100-0%	2C	2000	100% 0%	0.1Hz-5kHz	-
Wisconsin-Madison & McMaster [38]	n/a	18650	NCA	2018	25° 10° 0° -10° -20°	n/a	n/a	n/a	2900	100% 95% ... 5% 0%	1mHz-6kHz	-

Accessible data | Accessible but not for this project | Data not accessible

collected and how the EIS measurements were performed. N/a is used as *not available*.

4 Analysis Methodology

The main principles of the methodology algorithm in this paper are presented in Fig. 11, where the steps taken to process the impedance data in the ECM model are broken down. The model is based on the EIS measurement over a controlled ageing dataset of LIB as has been illustrated in Fig. 11(a). As shown in the visual representation of the processing algorithm, the paper's methodology focuses on three main stages. First, the results of the battery ageing from the EIS measurement, second the Distribution of Relaxation Times (DRT) analysis to deconvolute the EIS data during the whole battery ageing process, and finally, effective modelling with a proper ECM model and parametrization of the model. A similar approach has been proposed in [39]; in that case, correlating between battery ECM parameters as a function of open circuit voltage (OCV) has been investigated in different SOC and temperature. The algorithm is intended to process large amounts of data, and the selected dataset has over 20,000 EIS measurements.

4.1 Electrochemical Impedance Spectroscopy

EIS is a useful, non-destructive tool for analysing battery performance. By injecting a small AC sweep signal into the battery and measuring the resulting

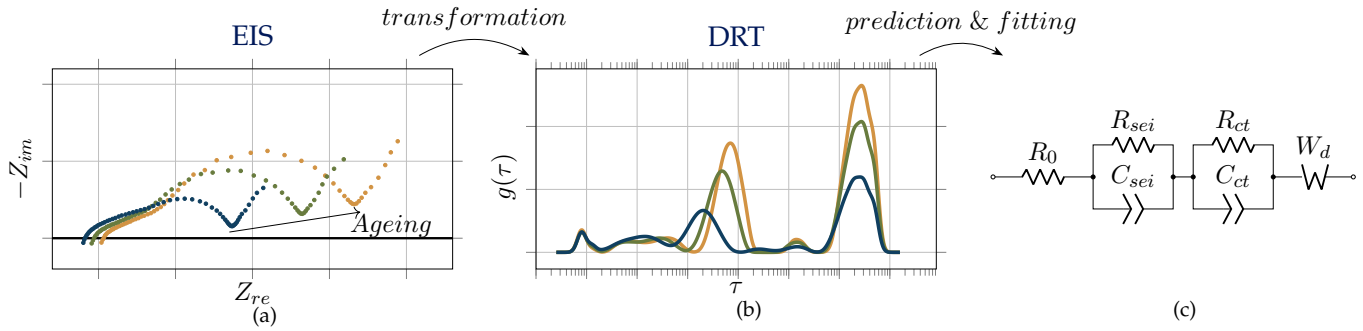

Fig. 11. Schematic overview of the steps in the proposed Electrical Equivalent Model (ECM) modelling methodology.

signal over a frequency range from mHz to kHz. Although EIS measurements are typically performed in a laboratory setting due to their complexity, they offer a valuable approach for developing models that can inform battery diagnostics and prognostics [40].

This process generates an impedance spectrum of the battery, which can be analysed and interpreted to gain a deeper understanding of the intricate electrochemical reactions occurring within the battery [41]. In Fig. 12, a typical EIS measurement is plotted in a Nyquist representation, with the different insights that can be gained from this measurement highlighted.

The impedance spectrum can be divided into several regions, each corresponding to different frequency ranges and providing specific information about the battery's performance and characteristics. In the low-frequency range, several phenomena can be observed, such as diffusion processes, charge transfer resistance, the presence of other semicircles, and the ohmic region.

The diffusion processes are related to the transport of ions and electrons within the battery's active materials. By analysing the low-frequency region, it is possible to determine the battery's diffusion limitations and gain insights into its capacity fade and rate capability.

The charge transfer resistance corresponds to the semicircle observed in the mid-frequency range. It is associated with the kinetics of electrochemical reactions at the electrode-electrolyte interface. Analysing this region can provide valuable information about the battery's performance under various operating conditions and help to identify potential degradation mechanisms.

Other semicircles that may appear in the impedance spectrum can be attributed to various interfacial reactions, such as side reactions or electrode film formation. These can significantly impact the battery's performance and lifetime, making their identification essential for proper battery management.

Finally, the ohmic region, observed in the high-frequency range, represents the battery's ohmic resistance, which includes the resistance of the electrolyte, current collectors, and other components. Analysing this region allows for the evaluation of the battery's internal resistance and potential issues related to temperature and ageing.

This process generates an impedance spectrum of the battery, which can be analysed and interpreted to gain a deeper understanding of the intricate electrochemical reactions occurring within the battery. In Fig. 12 it is shown a typical EIS measurement plotted in a Nyquist representation with the different insights you can gain from this measurement highlighted.

In this paper, we sequenced the dataset generated by the Cambridge university for the publication [21]. This dataset has been selected because, compared with other available EIS repositories, the data has enough resolution to extract features, up to 10 points per decade, ageing has been done at different temperatures and EIS measurements have been performed at each charging cycle of the battery.

From the EIS measurement, there are 2 parameters that can be extracted directly, which will be used later with the DRT values to fit the ECM circuit elements.

4.2 Distribution of Relaxation Times

When a change in potential or current perturbs an electrochemical system, the system will respond by redistributing charges and ions to reach a new equilibrium. The speed at which this redistribution occurs is determined by the rates of various chemical and electrochemical processes in the system.

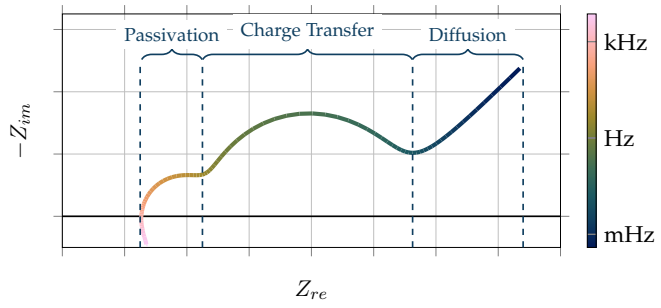

Fig. 12. Nyquist's visualization of an ideal EIS measurement. As a reference, the colormap shows the frequency at which each impedance feature is happening, allowing to attribute features to different processes inside the battery.

The DRT is a mathematical analysis technique used to extract information about the rates of these processes from the system's response to a perturbation. This is done by transforming the data from the frequency domain (f) to the time domain (τ). The result of the analysis will output a $g(\tau)$ values with peaks at certain, τ indicating an electrochemical process present [42].

Using only EIS measurements to analyse electrochemical systems can sometimes be misleading, as it can give the impression that the number of impedance elements in the system is different from it actually is. However, the DRT technique provides a more comprehensive and detailed analysis of the system's behaviour, allowing for a better understanding of the underlying chemical and electrochemical processes.

There are different algorithms proposed to compute this calculation such as Tikhonov Regularization [43]–[45], Maximum Entropy [46] or Fourier transform [47], [48]. in this project, we followed the algorithm proposed by [43] that follows the Tikhonov approach.

To achieve that, the experimental data is fitted against the Z_{DRT} model, which follows the expression:

$$Z_{DRT} = R_0 + \int_0^{\infty} \frac{g(\tau)}{1 + i2\pi f\tau} d\tau \tag{13}$$

where R_0 is the ohmic resistance, τ is the relaxation time, and $g(\tau)$ is the distribution function of relaxation times.

To obtain $g(\tau)$ from the measured impedance data, it needs to solve the inverse problem represented by equation 13. This is an ill-posed problem, which means that small errors in the input data may result in significant errors in the output. To overcome this issue, regularization techniques, such as Tikhonov regularization, the radial basis functions and the Dirac distribution.

Once $g(\tau)$ is known, the expression above can be discretized and normalized, ending up with the expression:

$$Z(\omega) = R_0 + R_{pol} \sum_{k=0}^{n} \frac{G(\tau_k)}{1 + j\omega\tau_k} \tag{14}$$

Being $\sum_{k=0}^{n} G(\tau_k) = 1$, the normalized version of $g(\tau)$. The $G(\tau)$, peaks of the $g(\tau)$ can be mapped over the impedance elements of the ECM with:

$$R_n = G(\tau_n) R_{pol} \tag{15}$$

$$C_n = {}^{R_n}/_{\tau_n} \tag{16}$$

or in case it opts for a R-CPE as the impedance element:

$$Q_n = (\frac{R_n}{\tau_n})^{\frac{1}{\alpha n}} \tag{17}$$

Even though one of the benefits introduced by the DRT is giving a model-free characterization of impedance spectra, this information should be analysed due to the fact that the data obtained is sensitive to the EIS quality and the tune of some DRT algorithm parameters [49]. In some papers like [39], [50] after performing the DRT analysis an RC value is mapped at every peak. This gives great accuracy, but when applying this technique to a whole dataset it introduces problems. False peaks may occur, as stated in [49], making the model not consistent through the ageing and difficulties within the task of tracking their differences. At the same time, choosing proper ECM needs an assumption of how the system behaves.

The proposed method to convert the DRT values into an ECM requirements taking into account the more prominent peaks that are present in all the datasets.

The peaks can be mapped to the RC networks proposed in suitable ECM, to choose the approximation that represents the best model, it is essential to know the application for which the model is designed.

A visual representation of the DRT analysis on an ideal EIS measurement can provide a better understanding of the process. In the Fig. 13 the DRT analysis had been made over the data of the ideal EIS measurement visualized on the Fig. 12.

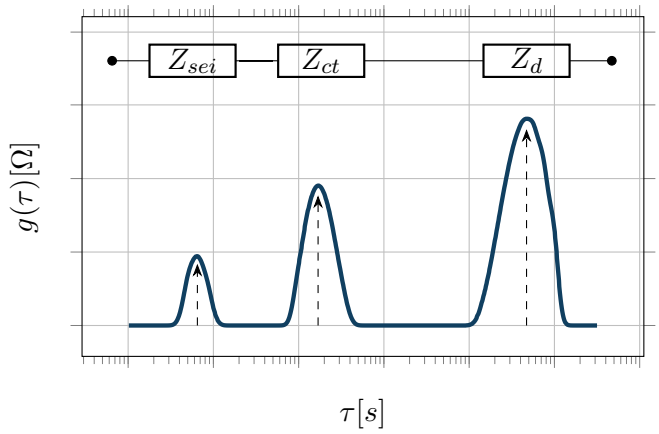

Fig. 13. DRT analysis of an ideal EIS measurement (solid line) giving the $g(\tau)$ values. The arrows mark the point where the main impedance characteristics are located, and the circuit above each peak is derived from the DRT shape. The exact shape of the ECM circuit will vary depending on the studied sample; for LIB, it is common to model each impedance element using R-C or R-CPE pairs respectively.

4.3 Equivalent Circuit Models

Accurately modelling battery ageing is essential for understanding the factors contributing to battery degradation and developing strategies to prolong battery life. EIS is a powerful tool for characterizing battery behaviour, as it can provide information about the battery's electrochemical properties and internal resistance. However, interpreting EIS data can be challenging due to the complex nature of the electrochemical processes occurring within a battery and the presence of noise and other sources of error in the measurements. This is where ECMs come into play - by offering a simplified representation of the battery's behaviour, they enable the extraction of useful information from EIS data and provide insights into the underlying mechanisms of battery ageing.

There are multiple approaches for selecting the appropriate form of the ECM. Fig. 14, adapted from [51], presents an ECM based on the physical construction of the cell, modelling different layers as distinct electrical components. This method is difficult to standardize, as it depends on the exact chemistry used for each layer, information that manufacturers rarely disclose. Furthermore, the complexity of this approach makes parameter calculation and maintaining linear ageing drift of the parameters challenging.

This phenomenon is caused by one of the disadvantages of ECMs: multiple parameter combinations can reproduce the same EIS shape, and this uncertainty is exacerbated by the number of parameters.

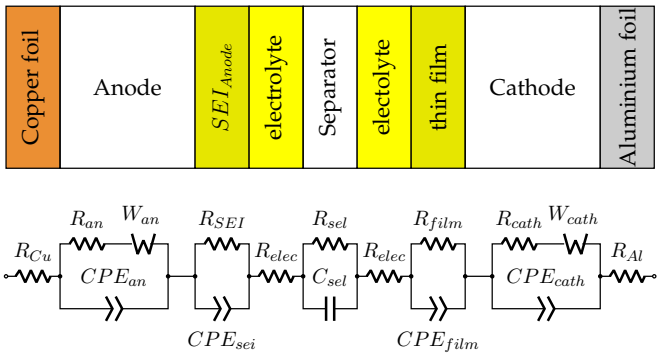

Fig. 14. Description of individual cell components with equivalent circuit elements, adapted from [51].

An alternative technique is to choose the circuit complexity based on the shape observed in the EIS measurements, with each semicircle modelled as an impedance element. In this work, we opted, as introduced in section 4.2, to determine the circuit shape by the features present in the EIS measurement, making this decision using the DRT to enhance the accuracy of the decision. This approach allows linking circuit elements with specific electrochemical processes that manifest in different regions of the EIS measurements, as discussed in section 4.1.

This modelling approach constructs the ECM from the regions of complex impedance present in the EIS, and that can be visualized in Fig. 12. These regions are linked to the frequency at which the measurements took place and are divided as:

- High frequencies: It encompasses the inductive behaviour, from the connections, cell geometry and cables [52], omitted in this work, and the ohmic resistance that models the resistivity of the electrolyte and electrodes[6].
- Mid-frequencies: Modelled as a series of parallel networks, usually as R-C pairs or R-CPE. In this region, it is manifested the effects of the charge transfer reactions and the double layer effect between the anode, cathode, and SEI.
- Low frequencies: This region is usually modelled as a Warburg element, a special case of CPE with a fixed phase angle of 45°. This region is attributed to the diffusion of the lithium-ions in the cell [53].

In this study, the EIS data indicated that the cells displayed three primary impedance phenomena, evidenced by two partly overlapping semicircles

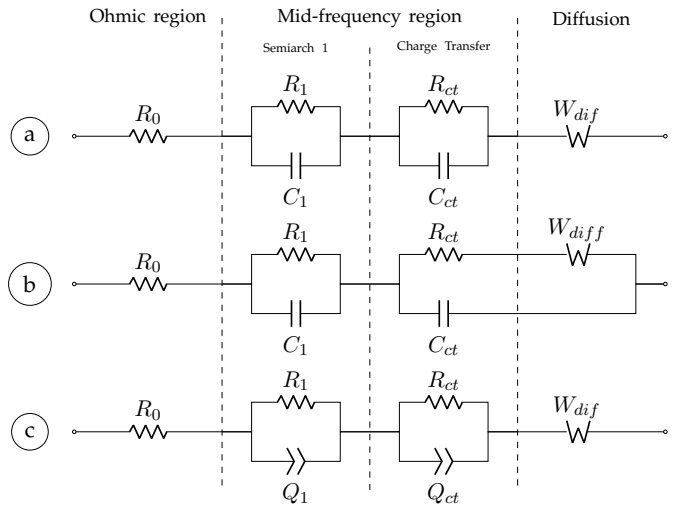

Fig. 15. Equivalent circuit models for three primary impedance processes, adapted from [56].

in the low and mid-frequency ranges, and a linear segment in the low-frequency range. This is similar to the shape observed in [54], where the high-to-middle frequency semicircle were related to lithium-ion migration through the SEI layer and surface film capacitance, while the low-frequency semicircle was associated with lithium-ion charge transfer, lithium-ion concentration in the electrolyte, and interfacial capacitance at the electrolyte interface. Furthermore, the inclined linear portion at very low frequencies signifies dominant mass transport and represents the controlled diffusion of electroactive species across the interface between surface films. To represent this shape, we chose one of the circuits depicted in Fig. 15 that could exemplify LIB cells with this arrangement.

The presented circuits are all valid models to accommodate data from LIB cells. The difference between them lies in their capacity to adapt to non-ideal data. Circuit A) has completely ideal semicircles centred in the real axis, while circuit C) uses the CPE element to allow more flexibility for the data to be fitted. Circuit B) is presented to show that the blocks that model each of the impedance features can be as complex as required, but with complexity comes an increase in the difficulty of fitting the values and calculating the initial values from the DRT analysis [54]–[57].

For our data sets, we decided to use circuit A) for the data obtained from the Cambridge data set and circuit C) for the data acquired in the U. Twente battery lab.

4.4 Accuracy comparison

The proposed method using the DRT modelling approach has an increase in the computation time of one to two seconds per each EIS measurement intended to analyse. That can add up when you are analysing from hundreds to thousands of measurements. But the benefits obtained with these methods can mitigate some of the problems that ECMs models have.

One of the major drawbacks that ECM models have is that different combinations of circuit values can produce the same impedance shape. Viewing it from the Least Squares Fit (LQF) algorithm means several minimums can be found. That can be seen in the data as the jittering in the errors, meaning that the algorithm is oscillating between different possible solutions between different runs.

With the DRT proposed approach is it possible to calculate good starting values to feed the LQF algorithm. This makes the algorithm start close to one of the minimums of the function and in consequent runs the algorithm will be tracking that specific minimum, making the error variability smaller.

This can be seen in Fig. 16, where a data set has been fitted to the same ECM, with and without the DRT process.

5 Results and Discussion

This section presents the analysis results of two datasets using the methodology described in Section 4.

As discussed in the section 3, there is the Cambridge data, collected on LR2032 Li-ion cells, and the dataset created in our group, collected over 18650 NMC cells. Since the datasets are from different cell types and chemistry and cycled on different cycling conditions, they can not be directly compared.

The dataset from the University of Cambridge has cells cycling at different temperatures, keeping all the other parameters constant. In contrast, the dataset from the University of Twente keeps the temperature constant, varying the discharging C-rate and the ΔDoD. Therefore, the results and the data analysis will be done in separate parts, and the results obtained will only reflect the conditions of each dataset.

Both datasets were processed following the methodology explained in section 4. Starting with an ageing EIS dataset with enough resolution, 10 points per decade, and in the frequency range between 10mHz to 20 kHz, the data is normalized

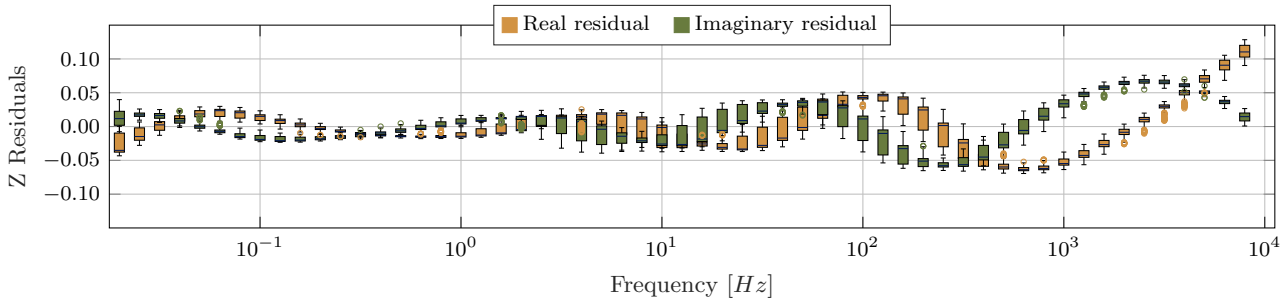

(a) Fitting data with DRT input

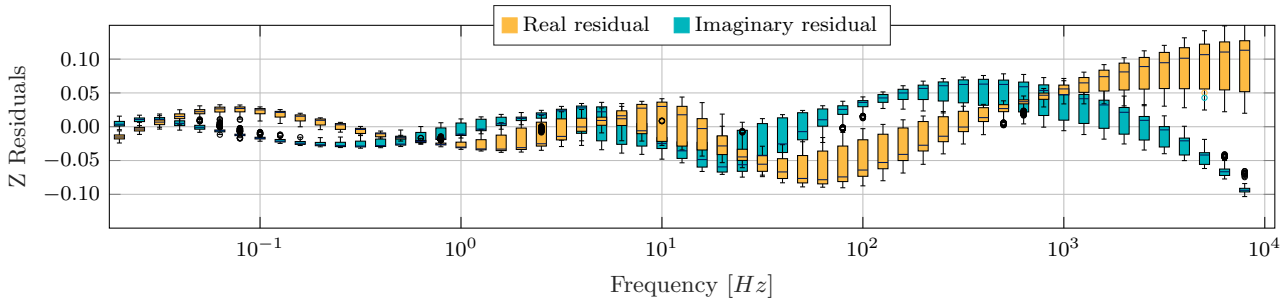

(b) Fitting data without DRT input

Fig. 16. Fit residual values of the real and imaginary parts of the Impedance residuals. The boxes represent the values within the first and third quartile of all the measurements taken in that frequency point, whereas the dark bar represents the median of that data. The x-axis is the frequency range studied, and the y-axis represents the relative error deviation. In the sub-figure (a) is the result after applying the DRT approach explained in this paper, and in the sub-figure (b) is the result after the same fitting process but skipping the DRT approach.

and processed with the DRT algorithm for each measurement point. From this first calculation it is extracted the shape of the ECM, selection of the observed peaks that are present in all the data, and using the values of these peaks to calculate a first approximation of the fitted values for the ECM. Then these values are processed using the LQF algorithm to adjust an ECM for each measurement point. Finally, the fitted values are compared with the dataset's ageing and conditions to try to find correlations between the drift of specific components with the cycling conditions.

5.1 Cambridge Dataset

5.1.1 Dataset selection and cleanup

The Cambridge dataset consists of 9 measurement points taken at various stages of the cycling profile and under different conditions. However, only sub-datasets I, V, and I were suitable for this project since they correspond to cells without any load and with a proper rest period. Sub-datasets II, III, VI, and VII were excluded since the measured impedance under load is non-linear. Sub-datasets IV and VIII were also excluded, as the cells had not reached electrochemical equilibrium after a rest period without load. We processed only sub-dataset V, as it corresponds to cells at charge, which are more stable and have a more linear measurement compared to sub-datasets I and IX. This section focuses on the ageing degradation of the cells, and thus, we did not consider the differences produced by the state of charge.

In Fig. 17, the capacity fade chart of the selected dataset can be seen. It can be appreciated that some cells had a short life span, not reaching 100 cycles, whereas all the others are aged to 250–300 cycles. In the original paper [21], those cells are omitted from the training dataset without a comment on the reason but considering the early decision on their EOL. The following results on the Cambridge dataset are based on cells 1, 2, and 3, aged at 25°; cells 1 and 2, aged at 35°; and cells 1 and 2, aged at 45°.

In Fig. 18, we can see the ageing drift measured over the cycles on one of the batteries that compose the dataset. The intention is to process the data to acquire an ECM and then try to find correlations with the ageing and, in this case, the temperature at which the cells were cycled. As a first observation, it can be seen that the majority of the differences

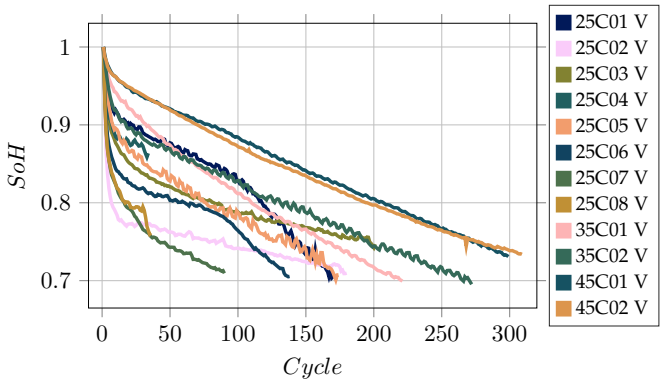

Fig. 17. Cambridge dataset SoH expressed as remaining capacity compared to the initial measurement.

induced by the ageing in the impedance can be observed in the mid to low frequencies, corresponding to the Charge Transfer and the Diffusion regions, as explained in section 4.1.

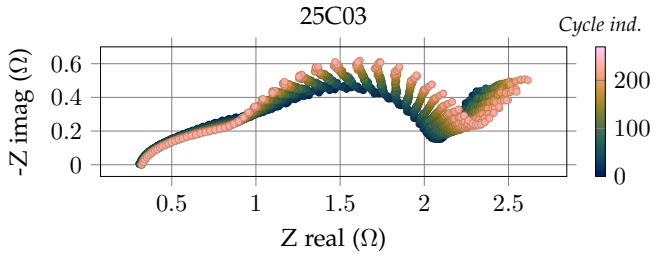

Fig. 18. EIS ageing on battery cell nr. 6 of Cambridge dataset. The colour is related to the cycle the measurement took place.

5.1.2 DRT: Peak selection and ECM

First, the EIS measurements were converted to DRT values using the Simple Run algorithm developed by [43], which requires impedance values and frequency information. It should be noted that the algorithm's performance is influenced by the sampling rate, with lower sampling rates leading to more erratic $g(\tau)$ values. In our dataset, we employed a sampling rate of 10 measurements per frequency decade (i.e., decade-by-decade sampling).

After processing the data, we obtained a distribution function of the RC pairs present in the dataset. For the ECM model, we selected the three most significant peaks from this distribution. The remaining two peaks had a relatively minor impact on the model, as their magnitudes were lower than the selected peaks, and their variance over the ageing was negligible.

To track the peaks, we employed a peak identification algorithm to extract the local peaks from the data. In the first sample, we manually selected the desired peaks. After that, a function was used to score the peaks in similarity to the selected peaks based on their distance and the expected ageing trend. From those scores, a new peak was selected for each initial peak. The process applied to the Cambridge dataset can be seen in Fig. 19.

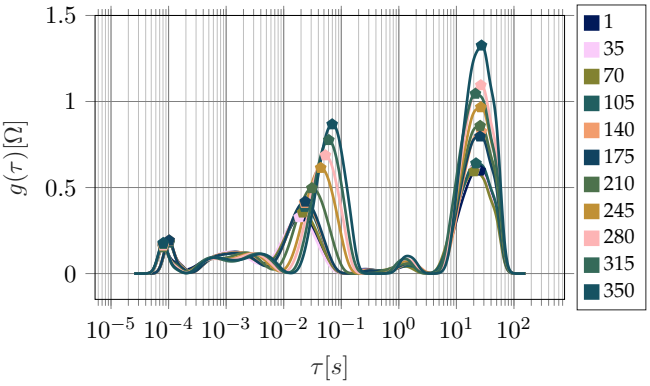

Fig. 19. Distribution of relaxation times at different cycle numbers of the Li-ion cell. The points mark the maximum of the selected impedance features in the Cambridge dataset for the cell 25C03.

5.1.3 Least Squares Fit

From the peaks selected above, and following the formula 15, 16 and 17, it is possible to calculate the ECM parameters from τ and G values. For the Q_x parameters, we assume an initial α value of 1, representing an ideal capacitor. Later the different R, C, Q, α and W components of the ECM are adjusted to the initial EIS measurement using the LQF algorithm. The LQF is sensitive to the initial parameters given to the system. In Fig. 20 it can be seen the difference between the measured impedance data of one EIS with the approximation extracted from the DRT and the final adjustment of the LQF. For the analysis of the Cambridge dataset, it was selected the shape

5.1.4 Data Correlations and Trends

In Tab. 2, we can see some of the fitted parameters we acquired, which is for one cell of the Cambridge data set.

The highest correlation is between the parameters of the Charge transfer and diffusion models. Specifically, the C_{ct} and R_{ct} parameters show a strong relationship. This is expected, as the elements modelling higher frequency impedance characteristics tend to remain constant across the ageing dataset.

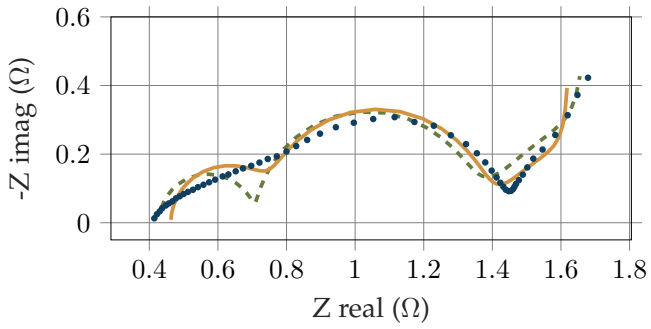

Fig. 20. Nyquist plot of cell 1 at 25 ℃ on cycle 120. Comparison between the measured impedance data (blue dots) and ECM model prediction, with the parameters directly extracted from the DRT (green line) and after LQF adjustment (yellow line).

TABLE 2
Values of the ECM parameters fitted with the DRT method as a function of ageing (cell cycling).

Cycle Nr	R_∞	R_a	C_a	R_b	C_b	W_c	W_c
	$[\Omega]$	$[\Omega]$	$[mF]$	$[\Omega]$	$[mF]$	$[\Omega]$	$[s]$
1	0.463	0.297	1.83	0.519	30.0	0.821	27.3
35	0.426	0.280	1.94	0.513	28.7	1.889	148
70	0.433	0.284	2.09	0.546	30.0	1.892	142.3
105	0.446	0.289	2.23	0.581	30.6	1.97	147.3
140	0.450	0.290	2.18	0.599	30.2	0.798	18.15
175	0.462	0.282	2.19	0.605	30.4	0.834	19.00
210	0.500	0.286	2.34	0.692	35.7	0.907	19.80
245	0.520	0.289	2.77	0.818	22.9	1.05	20.23
280	0.533	0.298	2.98	0.897	46.3	1.12	19.24
315	0.600	0.289	3.07	0.969	49.3	1.27	22.34
350	0.598	0.296	3.27	1.06	52.4	1.24	18.53

Fig.21 plots the C_{ct} and R_{ct} values, which show that the resistance in the charge transfer region is heavily influenced by temperature. As the ambient temperature during cycling increases, the resistivity increases at a faster rate. In contrast, the capacitance in the charge transfer region appears to be relatively insensitive to temperature differences and experiences similar depreciation across the different cycling conditions. The data present in the dataset had heavily differences from their starting impedance value. To eliminate the differences among the cells and focus on the ageing introduced by the cycling, the data has been normalized to the initial value calculated, showing the relative increase in their resistivity or capacitance.

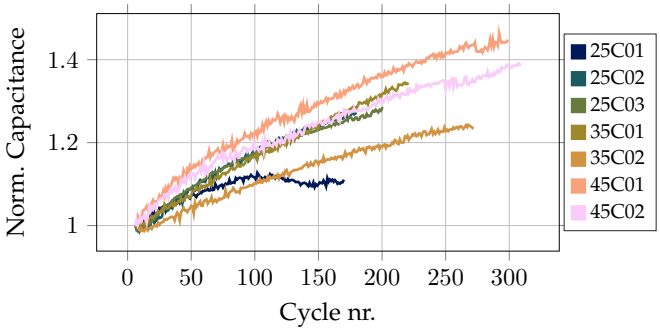

(a) Normalized C_{ct}

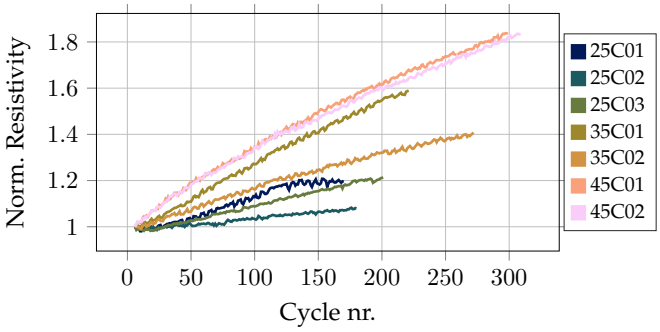

(b) Normalized R_{ct}

Fig. 21. Charge transfer impedance drift, divided into capacitance (a) and resistance (b). It can be seen that the resistance component of the Z_{ct} correlates with the temperature, whereas the capacitance increase is similar between the different temperatures.

5.2 Twente Dataset

5.2.1 *Dataset selection and cleanup*

The Twente dataset currently has 8 cells with EIS measurements at 0% SoC every ten cycles. As explained in Section 3.2.2 and, in more detail, in the Appendix A each cell is cycled at ambient temperature and at different ΔDoD and C-rates. In Fig. 22, the capacity fade chart of the dataset has been illustrated.

Observing Fig. 23(a), one can see that the impedance behaviour in the diffusion region, low frequency, has an unexpected shape. This unexpected behaviour is suspected to be caused by the electrochemical instability of low charge in the cell. At small frequencies, the measurement can be distorted by the AC signal that is induced in the cell to perform the EIS analysis. This introduced a problem as there is no ECM element that can mimic this frequency shape. With the inability to repeat the experiment in time, it was decided to continue the analysis with a filter in the data to exclude the

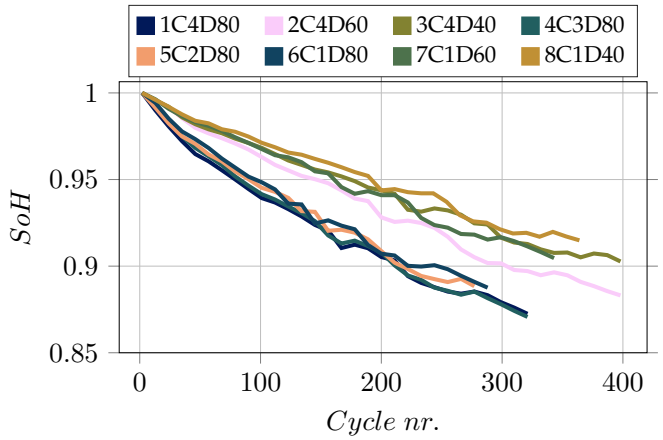

Fig. 22. University of Twente dataset SoH expressed as remaining capacity compared to the initial measurement.

diffusion layer. The cut-out frequency where the diffusion processes start to appear in the data is close to 10 mHz. In Fig. 23(b) one can see the ageing EIS measurements after the filtering process.

5.2.2 DRT: Peak selection and ECM

First, the EIS measurements were converted to DRT values using the Simple Run algorithm developed by [43], which requires impedance values and frequency information. It should be noted that the algorithm's performance is influenced by the sampling rate, with lower sampling rates leading to more erratic $g(\tau)$ values. In our dataset, we employed a sampling rate of 10 measurements per frequency decade (i.e., decade-by-decade sampling).

After processing the data, we obtained a distribution function of the RC pairs present in the dataset. For the ECM model, we selected the three most significant peaks from this distribution. The remaining two peaks had a relatively minor impact on the model, as their magnitudes were lower than the selected peaks, and their variance over the ageing was negligible.

To track the peaks, we employed a peak identification algorithm to extract the local peaks from the data. In the first sample, we manually selected the desired peaks. After that, a function was used to score the peaks in similarity to the selected peaks based on their distance and the expected ageing trend. From those scores, a new peak was selected for each initial peak.

The process applied to the Twente dataset can be seen in Fig. 24. With the frequency cut, only two peaks are visible and the third major impact that would be linked to the diffusion is omitted.

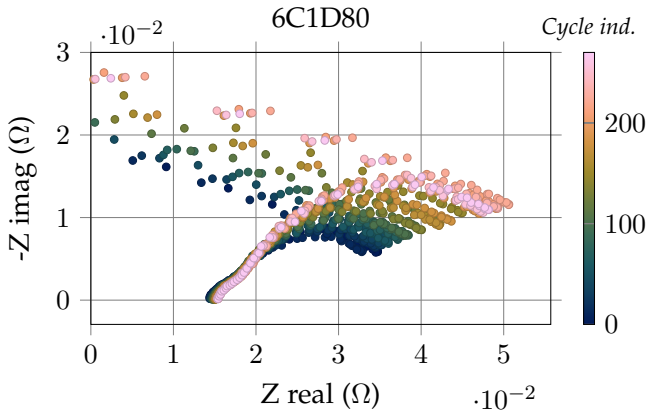

(a) Unfiltered Twente Dataset

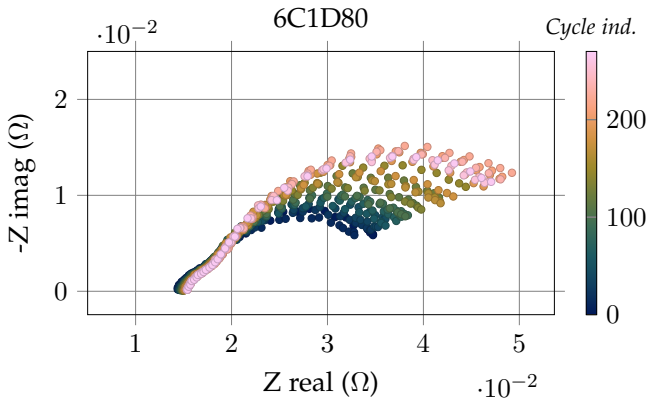

(b) Filtered Twente Dataset

Fig. 23. EIS ageing on battery cell nr. 6 of UT dataset. In a) before the filtering and in b) after the filtering of the diffusion region.

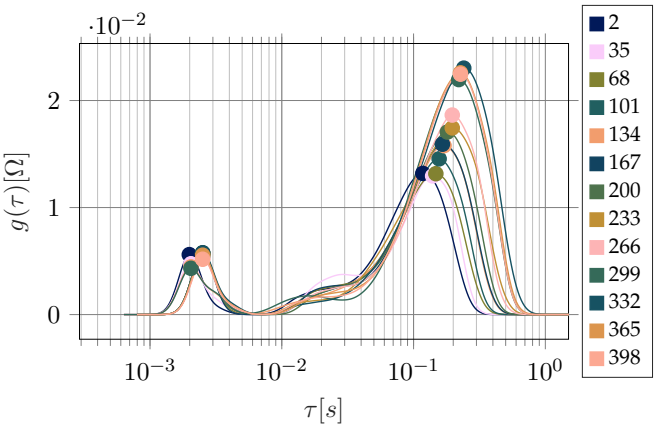

Fig. 24. Distribution of relaxation times at different cycle numbers of the Li-ion cell. The pints mark the maximum of the selected impedance features in the Twente dataset for the cell 6C1D80. This data has been filtered to discard the features at low frequencies/high τ.

5.2.3 Least Squares Fit

From the peaks selected above, and following the formula 15, 16 and 17, it is possible to calculate the ECM parameters from τ and G values. For the Q_x parameters, we are assuming an initial α value of 1, which represents an ideal capacitor. Later the different R, C, Q, α and W components of the ECM are adjusted to the initial EIS measurement using the LQF algorithm. The LQF is sensitive to the initial parameters given to the system. In Fig. 25 it can be seen the difference between the measured impedance data of one EIS with the approximation extracted from the DRT and the final adjustment of the LQF.

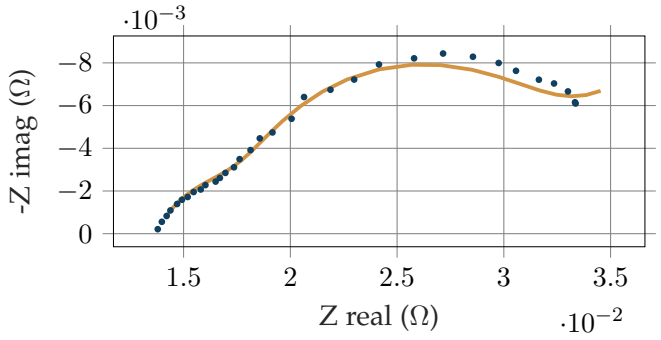

Fig. 25. Nyquist plot of cell 1C4D80 at the 2nd cycle. Comparison between the measured impedance data (blue dots) with the parameters after the DRT analysis and the LQF adjustment (yellow line).

5.2.4 Data Correlations and Trends

Analysing the results obtained in the Twente data set, we do not observe a meaningful correlation between the ageing process in the battery. As it can be seen in Fig. 26, only the fields that link the ageing with the cycling/State of Health (SoH) have any numerical significance.

This could be caused by two reasons. One possibility is that changes in the ΔDoD or the C-rate only have an effect on the capacity fade of the cell. As can be seen in Fig. 22 the cells cycled at 80% ΔDoD are fading faster than the cells cycled at 60% ΔDoD and those of the ones cycling at 40%. Another possibility could be that the distortion introduced by the measurement point, that has previously been discussed in the section 5.2.1, has an effect in other parts of the cells that affect the linearity of the measurements.

As shown in Fig. 27, the measurements exhibit some variability or jitter between consecutive measurement points. This behaviour was also observed in the Cambridge data set in the data measured at 0 SoC and the reason to decide to focus only on the measures taken at full charge.

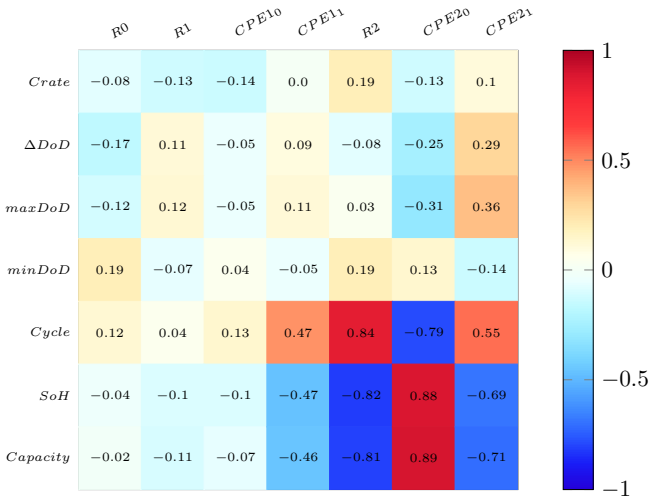

Fig. 26. Correlation Matrix of the different fitted values of the ECM with the characteristics of the cycling.

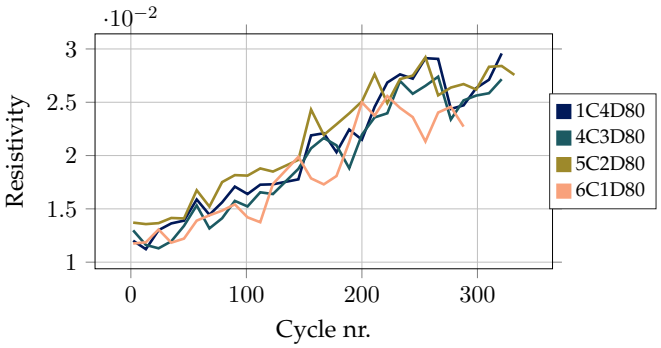

Fig. 27. R_{ct} changes over ageing at different C-rates and constant ΔDoD.

6 Conclusions

In this master thesis, we have investigated the ageing mechanisms of lithium-ion batteries. To do so, first, a search was made to gather and analyse all public datasets available and check for their relevance for the objectives and intend analysis of this project; the study and modelling of how the impedance change through the ageing of a cell and how is it related with the conditions of the environment where the cells are operating.

After identifying the knowledge gaps and common practices, an experiment was defined to complement the data available and enlarge the parameters where the cells are cycled on. To combine the different data sources, a common data structure was defined to accommodate the different repositories

and ease the analysis and possible comparability of the results.

Finally, an analysis methodology for large datasets has been proposed, combining long-standing analysis processes like ECM, whose efficacy has been widely acknowledged and documented, with new techniques as the DRT, that give an insight into the distribution of impedance processes present in the cells and allow the possibility to automate part of the analysis without losing accuracy in the process.

Following the proposed analysis methodology two different datasets had been analysed, the Cambridge dataset, the external open dataset that better fitted the data requirements of the proposed methodology, and the Twente dataset, the dataset that has been generated for this master thesis project. Between both datasets, there are represented different lithium-ion cell shapes, coin cells and 18650, chemistries NMC and LCO, and cycling conditions, different temperatures, C-rates and ΔDoD.

From the Cambridge dataset, the sub dataset V was processed. In it 12 cells are cycled at different temperatures, 25º,35º and 45º, maintaining all the other cycling conditions constant. With EIS measurements and capacity estimation being taken at each cycle. The data has been analysed with the proposed methodology. It has been found that the most prominent effect in the ageing is located in the mid to low frequencies, affecting the regions attributed to the charge transfer and the diffusion processes. From those, the real part of the impedance of the charge transfer region, modelled as a resistorR_{ct}, is heavily influenced by the cycling temperature, having a good correlation to the rate at which the resistivity increases with the cycling ambient temperatures of the cell with resistivity increasing at a faster rate as the ambient temperature increases. The other elements values remain mostly constant or don't show correlation with the different temperatures of the test.

In the Twente dataset we cycled 8 cells at room temperature, varying the ΔDoD at 80%, 60%, and 40% and the discharging C-rate at 1C, 2C, 3C, and 4C, while keeping all other cycling conditions constant throughout the ageing process of the cells. No correlation was observed between the EIS model parameters and the ageing process. This lack of correlation could be attributed to two primary reasons. First, it is possible that changes in the ΔDoD or C-rate predominantly affect the capacity fade of the cell, which was indeed observed in the capacity fade chart. These alterations might not have a significant impact on the ECM parameters, causing a weak or non-existent relationship between these factors and the ageing process. Second, the distortion introduced by the measurement point in the low-frequency region might affect the linearity of the measurements, thus impacting the observed correlations. Specifically, the problems encountered while measuring the cells at 0% SoC could have further complicated the analysis. At 0% SoC, the cells may exhibit non-linearities and higher noise levels, making it challenging to obtain accurate impedance measurements. Additionally, the low-frequency region is particularly susceptible to noise, drift, and other artefacts that could mask the true behaviour of the system, which in turn might influence the correlations observed.

The study has demonstrated the potential of using ECM parameters to understand the ageing mechanisms in lithium-ion batteries under different cycling conditions. However, certain limitations, such as the distortion in the measurements and the sensitivity of the LQF algorithm to initial parameters, should be addressed in future work. Further research can focus on developing more advanced ECMs and refining the methodology to provide better insights into the ageing process and battery performance.

7 Limitations and Recommendations

Data availability: One of the significant limitations of this study is the availability of high-quality battery datasets in the public domain. The scarcity of high-quality data can be attributed to various factors, including the proprietary nature of some datasets, insufficient documentation of experimental details that hinders the usability of the data, or the absence of key measurements relevant for this project such as EIS.

Data collection time requirements: Another significant limitation of this study is the time required to create a dataset that meets the necessary criteria. Cycling the cells and measuring their performance is time-consuming and resource-intensive. With only eight channels to cycle them in our lab there was a trade of between repeatability and difference in conditions that we could achieve; as the ageing process takes several months until the EOL point.

Experiment characteristics decisions: Due to the limited number of channels available to cycle the cells, only eight cycling conditions could be tested,

providing a limited sample size for each condition. This lack of replicates makes it challenging to assess the variability of the measured parameters. Additionally, we chose to perform the EIS measurements only at 0% SoC, which may not provide a complete understanding of the electrochemical processes occurring in the cell.

Addressing data availability issues:

Enlarge dataset experimentally Currently, the Twente Dataset has 8 cells. Firstly, it will be interesting to repeat the same experimental conditions while measuring the EIS at a different SoC to diminish the observed defects. This approach can help improve the accuracy and reliability of the data collected, and provide a better understanding of the impact of different SoC has on the impedance measurement and stability of the readings.

Next, expanding the dataset to include temperature variations would be valuable, as temperature is one of the factors with the most significant effects on ageing differences. Previous research has observed correlations between temperature and cell performance, and incorporating this variable into the dataset can provide more comprehensive insights into cell ageing processes.

Lastly, a potential avenue for future research is exploring the effect of emitted radiation on cell ageing, which is particularly relevant for the aerospace industry. Satellites and long-mission electronics are susceptible to space radiation, and understanding the impact of these conditions on cell ageing can contribute to the development of more resilient energy storage systems.

Enlarge dataset by collaborating with other institutions Collaborating with other universities and research institutions conducting similar research will be highly beneficial for future work. It may allow accessing a larger repository of information and open the possibility to define common experiment definition to increase the comparability among different studies. This will not only enhance the reliability and validity of the findings but also facilitate the identification of trends, patterns, and potential anomalies in the data.

Enlarge dataset by aligning experiments with published datasets Another possibility to enlarge the comparability of the collected data is to align the data produced with a public dataset, virtually enlarging the concluded experimented benefiting from previous work. This could be easily done to compare one chemistry with another one that was already tested by another university or, if it is possible to acquire the same cell, to test new cycling conditions in the same cell type.

Improving experiment design: Future research should focus on determining the optimal charge for measuring the cells, conducting a series of experiments at different SoC, and/or automating the data collection at different SoC points in the cycle. Incorporating temperature variations and radiation effects: Expanding the dataset to include temperature variations and exploring the effect of emitted radiation on cell ageing can provide more comprehensive insights into cell ageing processes.

ACKNOWLEDGMENTS

I would like to express my deepest gratitude to my daily supervisor, Seyedreza Azizighalehsari, for his support, guidance, and encouragement throughout this project. His expertise and mentorship have been invaluable.

I would also like to extend my heartfelt appreciation to prof.dr.ir. G. Rietveld, prof.dr. T. Batista Soeiro. and dr.ir. P. Venugopal, for their insightful feedback, constructive criticism, and patience. Their input has significantly contributed to the quality of this work.

Finally, I'd like to thank dr.ir. R.J.E. Hueting and ir. E. Molenkamp being part of my evaluation committee.

References

[1] B. Heid, M. Stuchte, and et al., "A vision for a sustainable battery value chain in 2030 unlocking the full potential to power sustainable development and climate change mitigation," *World Economic Forum*, Sep. 2019.

[2] J. Amici, P. Asinari, E. Ayerbe, and et al., "Inventing the sustainable batteries of the future," *Battery 2030+ Road Map*, Feb. 2022.

[3] M. Knipper, N. Ó Brolcháin, A. De Shryver, *et al.*, *State of the Art Report on Storage Technologies, Opportunities and Trends*, English, P. Mouratidis, Ed. Interreg North-West Europe, May 2021.

[4] S. Azizighalehsari, J. Popovic, P. Venugopal, and B. Ferreira, "A review of lithium-ion batteries diagnostics and prognostics challenges," in *IECON 2021 – 47th Annual Conference of the IEEE Industrial Electronics Society*, 2021, pp. 1–6. DOI: 10.1109/IECON48115.2021.9589204.

[5] N. Nitta, F. Wu, J. T. Lee, and G. Yushin, "Li-ion battery materials: Present and future," *Materials Today*, vol. 18, no. 5, pp. 252–264, 2015, ISSN: 1369-7021. DOI: https://doi.org/10.1016/j.mattod.2014.10.040. [Online]. Available: https://www.sciencedirect.com/science/article/pii/S1369702114004118.

[6] W. Waag, S. Käbitz, and D. U. Sauer, "Experimental investigation of the lithium-ion battery impedance characteristic at various conditions and aging states and its influence on the application," *Applied Energy*, vol. 102, pp. 885–897, 2013, Special Issue on Advances in sustainable biofuel production and use - XIX International Symposium on Alcohol Fuels - ISAF, ISSN: 0306-2619. DOI: https://doi.org/10.1016/j.apenergy.2012.09.030. [Online]. Available: https://www.sciencedirect.com/science/article/pii/S030626191200671X.

[7] M. E. Orazem and B. Tribollet, *Electrochemical Impedance Spectroscopy*, 2n. Wiley, 2017, ISBN: 978-1-119-36368-2.

[8] "Positive electrodes in lithium systems," in *Advanced Batteries: Materials Science Aspects*. Boston, MA: Springer US, 2009, ISBN: 978-0-387-76424-5. DOI: 10.1007/978-0-387-76424-5_9. [Online]. Available: https://doi.org/10.1007/978-0-387-76424-5_9.

[9] L. Croguennec and M. R. Palacin, "Recent achievements on inorganic electrode materials for lithium-ion batteries," *Journal of the American Chemical Society*, vol. 137, no. 9, pp. 3140–3156, 2015, PMID: 25679823. DOI: 10.1021/ja507828x. eprint: https://doi.org/10.1021/ja507828x. [Online]. Available: https://doi.org/10.1021/ja507828x.

[10] M. R. Palacin, "Battery materials design essentials," *Accounts of Materials Research*, vol. 2, no. 5, pp. 319–326, 2021. DOI: 10.1021/accountsmr.1c00026. eprint: https://doi.org/10.1021/accountsmr.1c00026. [Online]. Available: https://doi.org/10.1021/accountsmr.1c00026.

[11] J.-M. Tarascon and M. Armand, "Issues and challenges facing rechargeable lithium batteries," *Nature*, vol. 414, no. 6861, pp. 359–367, Nov. 2001, ISSN: 1476-4687. DOI: 10.1038/35104644. [Online]. Available: https://doi.org/10.1038/35104644.

[12] N. A. Kaskhedikar and J. Maier, "Lithium storage in carbon nanostructures," *Advanced Materials*, vol. 21, no. 25-26, pp. 2664–2680, 2009. DOI: https://doi.org/10.1002/adma.200901079. eprint: https://onlinelibrary.wiley.com/doi/pdf/10.1002/adma.200901079.

[13] Q. Li, J. Chen, L. Fan, X. Kong, and Y. Lu, "Progress in electrolytes for rechargeable li-based batteries and beyond," *Green Energy & Environment*, vol. 1, no. 1, pp. 18–42, 2016, ISSN: 2468-0257. DOI: https://doi.org/10.1016/j.gee.2016.04.006. [Online]. Available: https://www.sciencedirect.com/science/article/pii/S2468025716300218.

[14] P. Verma, P. Maire, and P. Novák, "A review of the features and analyses of the solid electrolyte interphase in li-ion batteries," *Electrochimica Acta*, vol. 55, no. 22, pp. 6332–6341, 2010, ISSN: 0013-4686. DOI: https://doi.org/10.1016/j.electacta.2010.05.072. [Online]. Available: https://www.sciencedirect.com/science/article/pii/S0013468610007747.

[15] M. M. Thackeray, "Manganese oxides for lithium batteries," *Progress in Solid State Chemistry*, vol. 25, no. 1, pp. 1–71, 1997, ISSN: 0079-6786. DOI: https://doi.org/10.1016/S0079-6786(97)81003-5. [Online]. Available: https://www.sciencedirect.com/science/article/pii/S0079678697810035.

[16] C. Masquelier and L. Croguennec, "Polyanionic (phosphates, silicates, sulfates) frameworks as electrode materials for rechargeable li (or na) batteries," *Chemical Reviews*, vol. 113, no. 8, pp. 6552–6591, Aug. 2013, ISSN: 0009-2665. DOI: 10.1021/cr3001862. [Online]. Available: https://doi.org/10.1021/cr3001862.

[17] X. Li, A. M. Colclasure, D. P. Finegan, *et al.*, "Degradation mechanisms of high capacity 18650 cells containing si-graphite anode and nickel-rich nmc cathode," *Electrochimica Acta*, vol. 297, pp. 1109–1120, 2019, ISSN: 0013-4686. DOI: https://doi.org/10.1016/j.electacta.2018.11.194. [Online]. Available: https://www.sciencedirect.com/science/article/pii/S0013468618326781.

[18] M. M. Doeff, "Battery cathodes," in *Batteries for Sustainability: Selected Entries from the Encyclopedia of Sustainability Science and Technology*, R. J. Brodd, Ed. New York, NY: Springer New York, 2013, pp. 5–49, ISBN: 978-1-4614-5791-6. DOI: 10.1007/978-1-4614-5791-6_2. [Online]. Available: https://doi.org/10.1007/978-1-4614-5791-6_2.

[19] R. Xiong, Y. Pan, W. Shen, H. Li, and F. Sun, "Lithium-ion battery aging mechanisms and diagnosis method for automotive applications: Recent advances and perspectives," *Renewable and Sustainable Energy Reviews*, vol. 131, p. 110 048, 2020, ISSN: 1364-0321. DOI: https://doi.org/10.1016/j.rser.2020.110048. [Online]. Available: https://www.sciencedirect.com/science/article/pii/S1364032120303397.

[20] G. dos Reis, C. Strange, M. Yadav, and S. Li, "Lithium-ion battery data and where to find it," *Energy and AI*, vol. 5, p. 100 081, 2021, ISSN: 2666-5468. DOI: https://doi.org/10.1016/j.egyai.2021.100081. [Online]. Available: https://www.sciencedirect.com/science/article/pii/S2666546821000355.

[21] Y. Zhang, Q. Tang, Y. Zhang, J. Wang, U. Stimming, and A. A. Lee, "Identifying degradation patterns of lithium ion batteries from impedance spectroscopy using machine learning," *Nature Communications*, vol. 11, no. 1,

p. 1706, Apr. 2020, ISSN: 2041-1723. DOI: 10.1038/s41467-020-15235-7.

[22] Y. Zhang, Q. Tang, Y. Zhang, J. Wang, U. Stimming, and A. A. Lee, *Identifying degradation patterns of lithium ion batteries from impedance spectroscopy using machine learning*, Zenodo, Feb. 2020. DOI: 10.5281/zenodo.3633835. [Online]. Available: https://doi.org/10.5281/zenodo.3633835.

[23] H. B. et al., *Battery cell testing data archive*, Sandia Lab, 2017. [Online]. Available: https://www.sandia.gov/ess/tools-resources/rd-data-repository.

[24] H. M. Barkholtz, A. Fresquez, B. R. Chalamala, and S. R. Ferreira, "A database for comparative electrochemical performance of commercial 18650-format lithium-ion cells," *Journal of The Electrochemical Society*, vol. 164, no. 12, A2697, Sep. 2017. DOI: 10.1149/2.1701712jes. [Online]. Available: https://dx.doi.org/10.1149/2.1701712jes.

[25] Y. Preger, H. M. Barkholtz, A. Fresquez, *et al.*, "Degradation of commercial lithium-ion cells as a function of chemistry and cycling conditions," *Journal of The Electrochemical Society*, vol. 167, no. 12, p. 120 532, Sep. 2020. DOI: 10.1149/1945-7111/abae37. [Online]. Available: https://dx.doi.org/10.1149/1945-7111/abae37.

[26] H. N. E. Institute and S. N. Labs, *Battery archive*, Hawai'i Natural Energy Institute and Sandia National Labs, Sep. 2020. [Online]. Available: www.batteryarchive.org.

[27] T. Raj, *Path dependent battery degradation dataset part 1*, university of Oxford, 2020. [Online]. Available: https://ora.ox.ac.uk/objects/uuid:de62b5d2-6154-426d-bcbb-30253ddb7d1e.

[28] T. Raj, *Path dependent battery degradation dataset part 2*, university of Oxford, 2020. [Online]. Available: https://ora.ox.ac.uk/objects/uuid:be3d304e-51fd-4b37-a818-b6fa1ac2ba9d.

[29] T. Raj, *Path dependent battery degradation dataset part 3*, university of Oxford, 2020. [Online]. Available: https://ora.ox.ac.uk/objects/uuid:78f66fa8-deb9-468a-86f3-63983a7391a9.

[30] G. Pozzato, A. Allam, and S. Onori, "Lithium-ion battery aging dataset based on electric vehicle real-driving profiles," *Data in Brief*, vol. 41, p. 107 995, 2022, ISSN: 2352-3409. DOI: https://doi.org/10.1016/j.dib.2022.107995. [Online]. Available: https://www.sciencedirect.com/science/article/pii/S2352340922002062.

[31] G. Pozzato, A. Allam, and S. Onori, *Lithium-ion battery aging dataset based on electric vehicle real-driving profiles*, OSF, Jul. 2022. [Online]. Available: https://osf.io/qsabn/?view_only=2a03b6c78ef14922a3e244f3d549de78.

[32] C. Pastor-Fernández, K. Uddin, G. H. Chouchelamane, W. D. Widanage, and J. Marco, "A comparison between electrochemical impedance spectroscopy and incremental capacity-differential voltage as li-ion diagnostic techniques to identify and quantify the effects of degradation modes within battery management systems," *Journal of Power Sources*, vol. 360, pp. 301–318, 2017, ISSN: 0378-7753. DOI: https://doi.org/10.1016/j.jpowsour.2017.03.042. [Online]. Available: https://www.sciencedirect.com/science/article/pii/S0378775317303269.

[33] C. Pastor-Fernández, T. Bruen, W. Widanage, M. Gama-Valdez, and J. Marco, "A study of cell-to-cell interactions and degradation in parallel strings: Implications for the battery management system," *Journal of Power Sources*, vol. 329, pp. 574–585, 2016, ISSN: 0378-7753. DOI: https://doi.org/10.1016/j.jpowsour.2016.07.121. [Online]. Available: https://www.sciencedirect.com/science/article/pii/S0378775316309995.

[34] C. Pastor-Fernandez, *Data for a comparison between electrochemical impedance spectroscopy and incremental capacity-differential voltage as li-ion diagnostic techniques to identify and quantify the effects of degradation modes within battery management systems*, University of Warwick, WMG, Aug. 2016. [Online]. Available: http://wrap.warwick.ac.uk/87247/.

[35] B. Saha and K. Goebel, *Battery data set*, NASA Prognostics Data Repository, NASA Ames Research Center, Sep. 2007. [Online]. Available: https://phm-datasets.s3.amazonaws.com/NASA/5.+Battery+Data+Set.zip.

[36] B. Bole, C. Kulkarni, and M. Daigle, *Randomized battery usage data set*, NASA Prognostics Data Repository, NASA Ames Research Center, Sep. 2007. [Online]. Available: https://phm-datasets.s3.amazonaws.com/NASA/11.+Randomized+Battery+Usage+Data+Set.zip.

[37] B. Bole, C. Kulkarni, and M. Daigle, "Adaptation of an electrochemistry-based li-ion battery model to account for deterioration observed under randomized use," Sep. 2014.

[38] P. J. Kollmeyer, "Panasonic 18650pf li-ion battery data," 2018.

[39] P. Iurilli, C. Brivio, R. E. Carrillo, and V. Wood, "Eis2mod: A drt-based modeling framework for li-ion cells," *IEEE Transactions on Industry Applications*, vol. 58, no. 2, pp. 1429–1439, 2022. DOI: 10.1109/TIA.2021.3134946.

[40] S. Azizighalehsari, P. Venugopal, D. P. Singh, and G. Rietveld, "Performance evaluation of retired lithium-ion batteries for echelon utilization," in *IECON 2022–48th Annual Conference of the IEEE Industrial Electronics Society*, IEEE, 2022, pp. 1–6.

[41] S. Azizighalehsari, P. Venugopal, D. P. Singh, M. Huijben, J. Popovic, and B. Ferreira, "High-performance lithium polymer battery pack for real-world racing motorcycle," in *2021 23rd European Conference on Power Electronics and Applications (EPE'21 ECCE Europe)*, IEEE, 2021, P–1.

[42] T. Paul, P. W. Chi, P. M. Wu, and M. K. Wu, "Computation of distribution of relaxation times by tikhonov regularization for li ion batteries: Usage of l-curve method," *Scientific Reports*, vol. 11, no. 1, p. 12 624, Jun. 2021, ISSN: 2045-2322. DOI: 10.1038/s41598-021-91871-3. [Online]. Available: https://doi.org/10.1038/s41598-021-91871-3.

[43] T. H. Wan, M. Saccoccio, C. Chen, and F. Ciucci, "Influence of the discretization methods on the distribution of relaxation times deconvolution: Implementing radial basis functions with drttools," *Electrochimica Acta*, vol. 184, pp. 483–499, 2015, ISSN: 0013-4686. DOI: https://doi.org/10.1016/j.electacta.2015.09.097. [Online]. Available: https://www.sciencedirect.com/science/article/pii/S0013468615305090.

[44] S. Dierickx, A. Weber, and E. Ivers-Tiffée, "How the distribution of relaxation times enhances complex equivalent circuit models for fuel cells," *Electrochimica Acta*, vol. 355, p. 136 764, 2020, ISSN: 0013-4686. DOI: https://doi.org/10.1016/j.electacta.2020.136764. [Online]. Available: https://www.sciencedirect.com/science/article/pii/S0013468620311579.

[45] A. Weiß, S. Schindler, S. Galbiati, M. A. Danzer, and R. Zeis, "Distribution of relaxation times analysis of high-temperature pem fuel cell impedance spectra," *Electrochimica Acta*, vol. 230, pp. 391–398, 2017, ISSN: 0013-4686. DOI: https://doi.org/10.1016/j.electacta.2017.02.011. [Online]. Available: https://www.sciencedirect.com/science/article/pii/S001346861730261X.

[46] T. Hörlin, "Deconvolution and maximum entropy in impedance spectroscopy of noninductive systems," *Solid State Ionics*, vol. 107, no. 3, pp. 241–253, 1998, ISSN: 0167-2738. DOI: https://doi.org/10.1016/S0167-2738(98)00008-3. [Online]. Available: https://www.sciencedirect.com/science/article/pii/S0167273898000083.

[47] B. A. Boukamp, "Derivation of a distribution function of relaxation times for the (fractal) finite length warburg.," *Electrochimica Acta*, vol. 252, pp. 154–163, 2017, ISSN: 0013-4686. DOI: https://doi.org/10.1016/j.electacta.2017.08.154. [Online]. Available: https://www.sciencedirect.com/science/article/pii/S0013468617318145.

[48] B. A. Boukamp and A. Rolle, "Analysis and application of distribution of relaxation times in solid state ionics," *Solid State Ionics*, vol. 302, pp. 12–18, 2017, ISSFIT12., ISSN: 0167-2738. DOI: https://doi.org/10.1016/j.ssi.2016.10.009. [Online]. Available: https://www.sciencedirect.com/science/article/pii/S0167273816304957.

[49] M. Hahn, S. Schindler, L.-C. Triebs, and M. A. Danzer, "Optimized process parameters for a reproducible distribution of relaxation times analysis of electrochemical systems," *Batteries*, vol. 5, no. 2, 2019, ISSN: 2313-0105. DOI: 10.3390/batteries5020043. [Online]. Available: https://www.mdpi.com/2313-0105/5/2/43.

[50] J. Xia, C. Wang, X. Wang, L. Bi, and Y. Zhang, "A perspective on drt applications for the analysis of solid oxide cell electrodes," *Electrochimica Acta*, vol. 349, p. 136 328, 2020, ISSN: 0013-4686. DOI: https://doi.org/10.1016/j.electacta.2020.136328. [Online]. Available: https://www.sciencedirect.com/science/article/pii/S0013468620307209.

[51] U. Westerhoff, K. Kurbach, F. Lienesch, and M. Kurrat, "Analysis of lithium-ion battery models based on electrochemical impedance spectroscopy," *Energy Technology*, vol. 4, no. 12, pp. 1620–1630, 2016. DOI: https://doi.org/10.1002/ente.201600154. eprint: https://onlinelibrary.wiley.com/doi/pdf/10.1002/ente.201600154. [Online]. Available: https://onlinelibrary.wiley.com/doi/abs/10.1002/ente.201600154.

[52] J. Schmitt, A. Maheshwari, M. Heck, S. Lux, and M. Vetter, "Impedance change and capacity fade of lithium nickel manganese cobalt oxide-based batteries during calendar aging," *Journal of Power Sources*, vol. 353, pp. 183–194, 2017, ISSN: 0378-7753. DOI: https://doi.org/10.1016/j.jpowsour.2017.03.090. [Online]. Available: https://www.sciencedirect.com/science/article/pii/S037877531730397X.

[53] S. Alavi, C. Birkl, and D. Howey, "Time-domain fitting of battery electrochemical impedance models," *Journal of Power Sources*, vol. 288, pp. 345–352, 2015, ISSN: 0378-7753. DOI: https://doi.org/10.1016/j.jpowsour.2015.04.099. [Online]. Available: https://www.sciencedirect.com/science/article/pii/S0378775315007569.

[54] Y. L. Cheah, N. Gupta, S. S. Pramana, V. Aravindan, G. Wee, and M. Srinivasan, "Morphology, structure and electrochemical properties of single phase electrospun vanadium pentoxide nanofibers for lithium ion batteries," *Journal of Power Sources*, vol. 196, no. 15, pp. 6465–6472, 2011, ISSN: 0378-7753. DOI: https://doi.org/10.1016/j.jpowsour.2011.03.039. [Online]. Available: https://www.sciencedirect.com/science/article/pii/S0378775311006549.

[55] Q.-A. Huang, Y. Shen, Y. Huang, L. Zhang, and J. Zhang, "Impedance characteristics and diagnoses of automotive lithium-ion batteries at 7.5% to 93.0% state of charge," *Electrochimica Acta*, vol. 219, pp. 751–765, 2016, ISSN: 0013-4686. DOI: https://doi.org/10.1016/j.electacta.2016.09.154. [Online]. Available: https://www.sciencedirect.com/science/article/pii/S0013468616320850.

[56] P. Iurilli, C. Brivio, and V. Wood, "On the use of electrochemical impedance spectroscopy to characterize and model the aging phenomena of lithium-ion batteries: A critical review," *Journal of Power Sources*, vol. 505, p. 229 860, 2021, ISSN: 0378-7753. DOI: https://doi.org/10.1016/j.jpowsour.2021.229860. [Online]. Available: https://www.sciencedirect.com/science/article/pii/S0378775321003992.

[57] S. Zhang, K. Xu, and T. Jow, "Eis study on the formation of solid electrolyte interface in li-ion battery," *Electrochimica Acta*, vol. 51, no. 8, pp. 1636–1640, 2006, Electrochemical Impedance Spectroscopy, ISSN: 0013-4686. DOI: https://doi.org/10.1016/j.electacta.2005.02.137. [Online]. Available: https://www.sciencedirect.com/science/article/pii/S0013468605007966.

APPENDIX A
EXPERIMENTAL SET-UP

A.1 Tested battery

The commercial 18650 cell studied was selected following the criteria of being manufactured by a reputable manufacturer, to guarantee a consistency between different cells. Having a chemistry popular in the automotive industry and allowing high current capabilities. After reviewing different candidates and consulting their availability, the NMC cell from Murata was selected.

In the table 3 there are listed additional specifications of the selected cell.

TABLE 3
Technical specifications US18650TC5A cell

Manufacturer	Sony / Murata
Model	US18650TC5A
Positive electrode	$LiNiMnCoO_2$
Negative electrode	Carbon
Diameter	18.20 mm
Length	64.95 mm
Weight	47.8g
Nominal capacity	2600mAh
Nominal voltage	3.6V
Charge cut-off voltage	4.2V
Discharge cut-off voltage	2.0V
Continuous discharge current	25A
Constant charge current, max.	6.0A
Constant charge current, recommended	2.5A

A.2 Cycling equipment

The lab arrangement can be seen in the figure 28. The cycling protocol was carried out using the Arbin battery cycler model LBT21084HC. The individual cells tested were placed in the 30A kelvin clamps also from Arbin. The EIS measurements were taken using the *Interface 5000E* potentiostat/galvanostat from Gamry. Each cell was thermally monitored using the TC-08 Thermocouple data logger from PicoLog. The climatic chamber was not used for this data collection.

A.3 Cycling protocol

At the beginning of the test, a formation cycle was performed on all the cells. This consisted in a CC-CV charging followed by a CC $\frac{C}{10}$ discharge. This is done to stabilize the SEI formation and assure

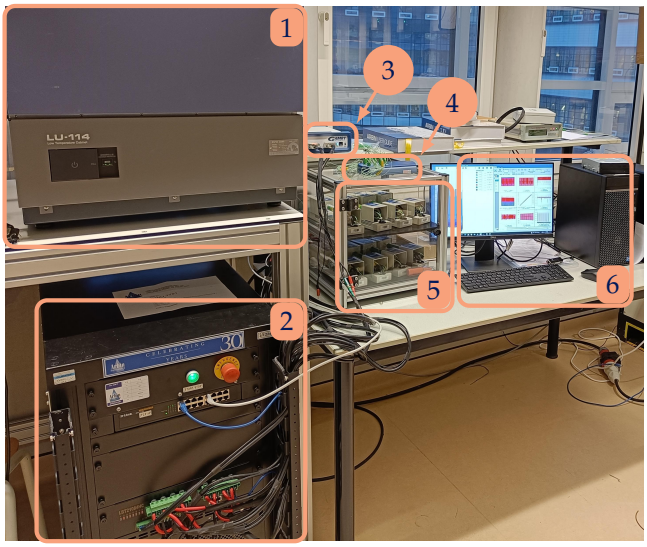

Fig. 28. Test Equipment. 1)Climatic chamber... 2)Arbin LBT 5V-30A-8CH 3)Gamry Interface 5000E 4)TC-08 Thermocouple data logger 5)Battery Holders and cells 6) Computer running MITS Pro 8 software (controlling the experiment)

that all the cells start the cycling under the same condition.

Each round of cycling starts with an internal resistance measurement, followed by a capacity estimation cycle, an EIS measurement and, in this case, 10 ageing cycles at the designated conditions. After that, if the cell falls under the determined EOL of 80% of its SoH the experiment is considered over. In the contrary, the cell starts another cycling round. As can be seen in the figure 22 in the partial data extraction presented in this project, none of the cells reached the end of the experiment and are still cycling.

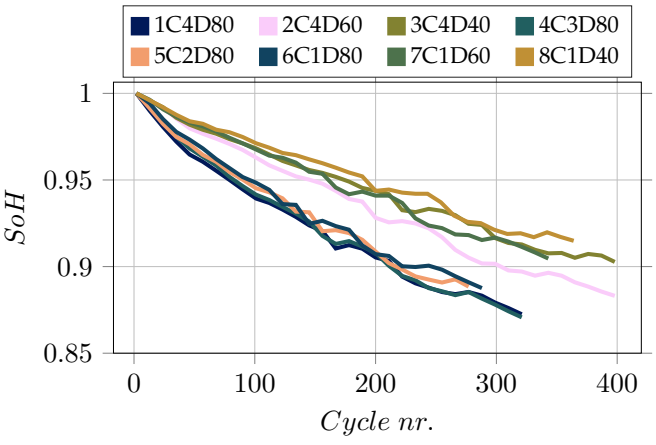

Fig. 29. capacity fade UT

The capacity estimation was performed doing a 100% SoC in 1C CC-CV followed by a 0.5C CC

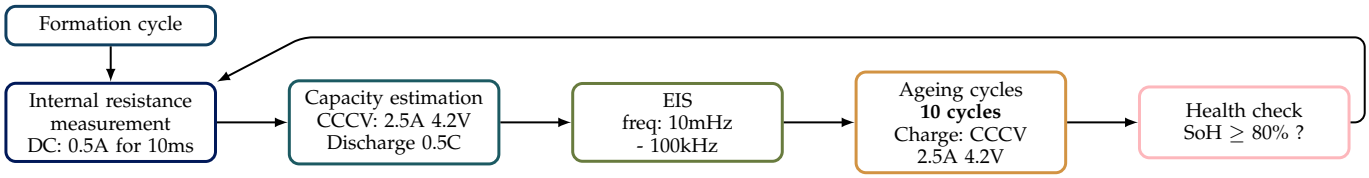

Fig. 30. Cycling ageing protocol

discharge till the established 0% SoC defined by the manufacturer as a voltage limit. The accumulated discharge of the battery in this cycle is considered the current maximum charge of the cell. This value compared with the first recorded maximum charge is used as the SoH indicator and is used for the EOL condition.

The table 4 resumes the different cycling conditions examined. All cells were cycled in ambient temperature and thermally monitored to assure the cells don't operate over the manufacturer limits.

The nominal capacity of the cells were used for calculating C-rates, that in this experiment can be 1C, 2C, 3C and 4C. All cells were charged at a rate of 1C, as stated by the manufacturer. The second cycling condition investigated in this experiment was the effect in the ΔDoD. Three different were considered, 40% cycling from 40% to 80% SoC; 60%, cycling form 20% to 80% SoC and 80% ΔDoD, cycling from 20% to 100% SoC.

The cells cycling till 100% SoC were cycled using the CC-CV protocol. For partial charges, only constant-current was used, as it is estimated that the transition from constant current to constant voltage occurs around 95% of SoC.

TABLE 4
Cycling

$C\,rate$ \ ΔDoD	20% - 100%	20%- 80%	40% - 80%
4C	CH1	CH2	CH3
3C	CH4	-	-
2C	CH5	-	-
1C	CH6	CH7	CH8